Article

NINJ1 mediates plasma membrane rupture during lytic cell death

https://doi.org/10.1038/s41586-021-03218-7

Received: 20 August 2020

Accepted: 11 January 2021

Published online: 20 January 2021

Check for updates

Nobuhiko Kayagaki[1]✉, Opher S. Kornfeld[1], Bettina L. Lee[1], Irma B. Stowe[1], Karen O'Rourke[1], Qingling Li[2], Wendy Sandoval[2], Donghong Yan[3], Jing Kang[3], Min Xu[3], Juan Zhang[3], Wyne P. Lee[3], Brent S. McKenzie[3], Gözde Ulas[4], Jian Payandeh[5], Merone Roose-Girma[6], Zora Modrusan[2], Rohit Reja[7], Meredith Sagolla[8], Joshua D. Webster[8], Vicky Cho[9,10], T. Daniel Andrews[10], Lucy X. Morris[9], Lisa A. Miosge[9,10], Christopher C. Goodnow[11,12], Edward M. Bertram[9,10] & Vishva M. Dixit[1]✉

Plasma membrane rupture (PMR) is the final cataclysmic event in lytic cell death. PMR releases intracellular molecules known as damage-associated molecular patterns (DAMPs) that propagate the inflammatory response[1–3]. The underlying mechanism of PMR, however, is unknown. Here we show that the cell-surface NINJ1 protein[4–8], which contains two transmembrane regions, has an essential role in the induction of PMR. A forward-genetic screen of randomly mutagenized mice linked NINJ1 to PMR. *Ninj1*$^{-/-}$ macrophages exhibited impaired PMR in response to diverse inducers of pyroptotic, necrotic and apoptotic cell death, and were unable to release numerous intracellular proteins including HMGB1 (a known DAMP) and LDH (a standard measure of PMR). *Ninj1*$^{-/-}$ macrophages died, but with a distinctive and persistent ballooned morphology, attributable to defective disintegration of bubble-like herniations. *Ninj1*$^{-/-}$ mice were more susceptible than wild-type mice to infection with *Citrobacter rodentium*, which suggests a role for PMR in anti-bacterial host defence. Mechanistically, NINJ1 used an evolutionarily conserved extracellular domain for oligomerization and subsequent PMR. The discovery of NINJ1 as a mediator of PMR overturns the long-held idea that cell death-related PMR is a passive event.

Pyroptosis is a potent inflammatory mode of lytic cell death triggered by diverse infectious and sterile insults[2,3,9]. It is driven by the pore-forming fragment of gasdermin D (GSDMD)[10–13] and releases two exemplar proteins: the pro-inflammatory cytokine IL-1β, and LDH, a standard marker of PMR and lytic cell death. An early landmark study[14] predicted two sequential steps for pyroptosis: (1) initial formation of a small plasma membrane pore that causes the release of IL-1β and non-selective ionic fluxes, and (2) subsequent PMR attributable to oncotic cell swelling. PMR releases LDH (140 kDa) and large DAMPs. Although the predicted size of gasdermin pores (approximately 18 nm inner diameter[15]) is large enough to release IL-1β (17 kDa, around 4.5 nm diameter), the underlying mechanism for subsequent PMR has been considered a passive osmotic lysis event.

A forward-genetic screen identifies NINJ1

To identify essential mediators of PMR, we performed a forward-genetic screen using bone marrow-derived macrophages (BMDMs) from mice mutagenized with *N*-ethyl-*N*-nitrosourea (ENU). Cytoplasmic lipopolysaccharide (LPS), a potent stimulator of the non-canonical inflammasome, was used to initiate caspase-11- and GSDMD-dependent release of LDH[10,11] from BMDMs that were primed with the Toll-like receptor 2 (TLR2) agonist Pam3CSK4. Mice derived from pedigree IGL03767 exhibited a Mendelian-recessive trait that compromised LDH release (Fig. 1a). Exome sequencing of the founder G1 male identified 19 single nucleotide variants (SNVs). Subsequent phenotyping and SNV genotyping showed that the trait correlated with inheritance of a point mutation in the gene encoding NINJ1 (Extended Data Fig. 1a, b, Extended Data Table 1).

NINJ1 is a 16-kDa cell-surface protein that has two transmembrane regions with N and C termini outside the cytoplasm (N_{out}/C_{out} topology) (Fig. 1b). NINJ1 is widely expressed, including in myeloid cells and the central nervous system, and reportedly functions as an adhesion molecule that is associated with inflammation and tumour suppression[4–8]. The SNV (A→T) occurred at the non-coding 3′ splice acceptor site of exon 2 (Extended Data Fig. 1c). Accordingly, the 16-kDa NINJ1 protein detected in wild-type BMDMs was absent in mutant *Ninj1*$^{mt/mt}$ BMDMs (Fig. 1c). NINJ1 deficiency attenuated GSDMD-dependent LDH

[1]Department of Physiological Chemistry, Genentech Inc., South San Francisco, CA, USA. [2]Department of Microchemistry, Proteomics and Lipidomics, Genentech Inc., South San Francisco, CA, USA. [3]Department of Translational Immunology, Genentech Inc., South San Francisco, CA, USA. [4]Department of Biochemical and Cellular Pharmacology, Genentech Inc., South San Francisco, CA, USA. [5]Department of Structural Biology, Genentech Inc., South San Francisco, CA, USA. [6]Department of Molecular Biology, Genentech Inc., South San Francisco, CA, USA. [7]Department of Bioinformatics, Genentech Inc., South San Francisco, CA, USA. [8]Department of Pathology, Genentech Inc., South San Francisco, CA, USA. [9]The Australian Phenomics Facility, The John Curtin School of Medical Research, The Australian National University, Canberra, Australian Capital Territory, Australia. [10]Department of Immunology and Infectious Diseases, The John Curtin School of Medical Research, The Australian National University, Canberra, Australian Capital Territory, Australia. [11]Garvan Institute of Medical Research, Sydney, New South Wales, Australia. [12]Cellular Genomics Futures Institute, UNSW Sydney, Sydney, New South Wales, Australia. ✉e-mail: kayagaki@gene.com; dixit@gene.com

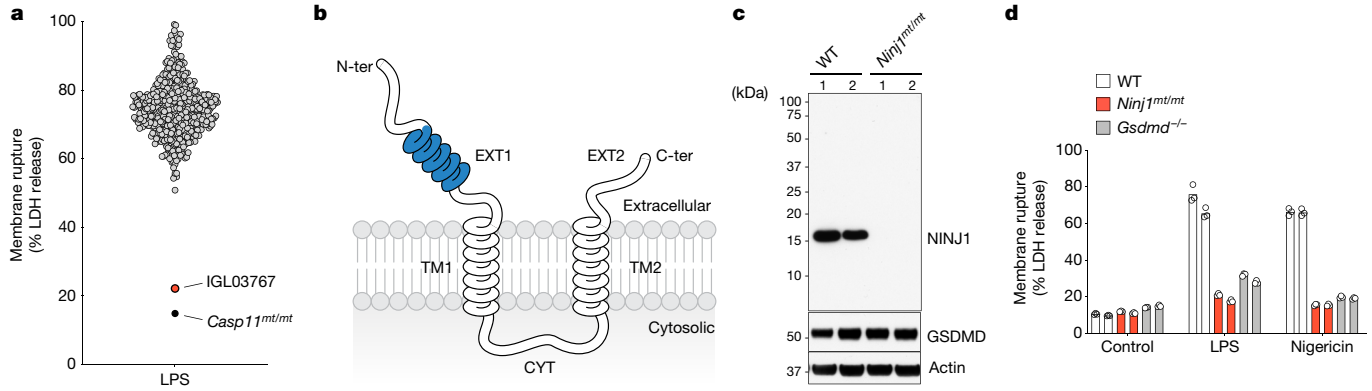

Fig. 1 | Forward genetic screen identifies a mutation in *Ninj1* that abolishes PMR. a, Screening of third-generation (G3) offspring from C57BL/6 mice treated with ENU. Graph shows LDH released from BMDMs primed with the TLR2 agonist Pam3CSK4 after LPS electroporation. Red dot represents IGL03767 G3 7 (Extended Data Fig. 1a, b). Grey dots represent other G3 mice in the same batch from multiple pedigrees. Black, *Casp11*$^{mt/mt}$ 129X1/SvJ mouse (*Casp11* is also known as *Casp4*). **b**, Predicted structure of NINJ1. Blue, extracellular α-helix domain. CYT, cytoplasmic region; EXT, extracellular region; TM, transmembrane domain. **c**, Immunoblot of NINJ1 from BMDM extracts. Lane numbers indicate different mice. $n = 2$ per genotype. WT, wild type. **d**, LDH released from primed BMDMs stimulated with LPS electroporation or nigericin. Control denotes medium alone. Data are means (bars) of at least three individual replicates (circles). $n = 2$ per genotype. For gel source data, see Supplementary Fig. 1.

release in response to either LPS or nigericin (an ionophore activator of the NLRP3 canonical inflammasome)[10,11,16] (Fig. 1d).

NINJ1 is essential for pyroptosis-related PMR

Similar to *Ninj1*$^{mt/mt}$ BMDMs, *Ninj1*$^{-/-}$ and *Gsdmd*$^{-/-}$ BMDMs released less LDH than wild-type BMDMs in response to treatment with LPS or nigericin, or infection with *Salmonella* Typhimurium, *Escherichia coli* or *C. rodentium* (Fig. 2a, Extended Data Fig. 2a). We further assessed PMR by time-lapse live-cell imaging of BMDMs preloaded with large dextran dyes (dextran dye conjugates of 150 or 70 kDa, hereafter termed DD-150 or DD-70). LPS triggered less release of dextran dye from *Ninj1*$^{-/-}$ BMDMs than from wild-type BMDMs (Fig. 2b). Exogenous expression of NINJ1 in *Ninj1*$^{-/-}$ immortalized macrophages (iMACs) restored LPS-induced release of DD-150 (Extended Data Fig. 2b), supporting a crucial role for NINJ1 in PMR. By contrast, NINJ1 deficiency did not impair the GSDMD-dependent release of a smaller dye (DD-3) or the intake of the 1.2-kDa cell-impermeable dye YOYO-1 (Fig. 2b). Thus, the formation of GSDMD pores appears intact in *Ninj1*$^{-/-}$ BMDMs. Consistent with this notion, wild-type and *Ninj1*$^{-/-}$ BMDMs both produced the N-terminal pore-forming fragment of GSDMD[10–13] in response to treatment with either nigericin or cytoplasmic LPS (Fig. 2c, Extended Data Fig. 2c). Collectively, these data reveal that NINJ1 is crucial for PMR, but dispensable for the formation of GSDMD pores.

IL-1β is a hallmark cytokine for pyroptosis that is thought to exit dying BMDMs through the GSDMD pore[2,3,9,14,15]. Accordingly, wild-type and *Ninj1*$^{-/-}$ BMDMs released comparable levels of IL-1β in response to either nigericin or cytoplasmic LPS (Fig. 2d). NINJ1 was also dispensable for the release of IL-18, another pyroptosis-associated IL-1 family member (Extended Data Fig. 2d). Wild-type and *Ninj1*$^{-/-}$ BMDMs were mostly indistinguishable in transcriptomic analyses, lipid composition, and TLR-induced production of IL-6 and TNF (Extended Data Fig. 2e–g). In summary, our data provide compelling genetic evidence that the release of IL-1β and IL-18 from macrophages is independent of PMR and probably occurs via the approximately 18-nm GSDMD pore.

Wild-type BMDMs stimulated with either nigericin or cytoplasmic LPS undergo characteristic morphological changes during pyroptosis; the cells cease moving, swell and develop bubble-like herniations that disintegrate abruptly to yield a shrunken corpse[2,14,17]. NINJ1 deficiency inhibited bubble disintegration while upstream events were unaltered (Fig. 2e, f, Supplementary Videos 1–3). Remarkably, even at 16 h after exposure to LPS or nigericin, *Ninj1*$^{-/-}$ BMDMs retained prominent 'bubble' morphology (Fig. 2e). The cells were dead based on their loss of ATP, mitochondrial membrane potential, and motility (Fig. 2g, Extended Data Fig. 2h, Supplementary Videos 1, 2). Thus, PMR and related events, including LDH release and bubble disintegration, are genetically separable from GSDMD-driven cell death and IL-1β release. PMR is probably an event that occurs after cell death[17,18]. Of note, BMDMs ceased moving before bubble formation (Supplementary Videos 1, 2). NINJ1-independent loss of mitochondrial membrane potential also preceded PMR (as assessed by release of DD-150) (Extended Data Fig. 2h, i).

We confirmed that NINJ1-mediated PMR released more proteins than just LDH. Supernatants from wild-type BMDMs stimulated with nigericin or cytoplasmic LPS contained many proteins that were diminished in their *Ninj1*$^{-/-}$ counterparts (Fig. 2h, Extended Data Fig. 2j). Subsequent secretome analysis detected approximately 780 molecules (including plectin) that were released in a NINJ1-dependent manner in response to cytoplasmic LPS (Fig. 2i, Extended Data Table 2). Of note, *Ninj1*$^{-/-}$ BMDMs were unable to release HMGB1, a proinflammatory DAMP[19], despite exhibiting normal GSDMD-dependent release of IL-1α (Fig. 2j, k). HMGB1 is a relatively small nuclear protein of approximately 28-kDa, but forms large complexes with nucleosomes and transcription factors[20], which probably hinders its release through the approximately 18-nm GSDMD pore. Regardless, the NINJ1-dependent release of diverse intracellular proteins from pyroptotic cells, including HMGB1, suggests a pro-inflammatory role of NINJ1. Indeed, *Ninj1*$^{-/-}$ mice were more susceptible than wild-type mice to infection with *C. rodentium* (Fig. 2l). Thus, NINJ1-dependent PMR may release DAMPs that are important for host defence against bacteria. *Ninj1*$^{-/-}$ mice exhibited normal susceptibility to caspase-11-dependent[16] and GSDMD-dependent[11] acute septic shock induced by LPS (Extended Data Fig. 2k), which suggests that mechanisms that are driven by GSDMD but independent of PMR promote LPS-induced mortality.

NINJ1 has a global role in PMR

PMR is not exclusive to pyroptosis, and also occurs during necrosis or post-apoptosis (sometimes referred to as secondary necrosis)[21]. We examined the role of NINJ1 in non-pyroptotic PMR. In control experiments, pyroptotic stimuli (such as cytoplasmic LPS, nigericin and flagellin[10,11]) caused NINJ1- and GSDMD-dependent PMR in BMDMs on the basis of LDH release, whereas PMR after freezing and thawing of cells did not require NINJ1 (Fig. 3a). *Ninj1*$^{-/-}$ BMDMs released less

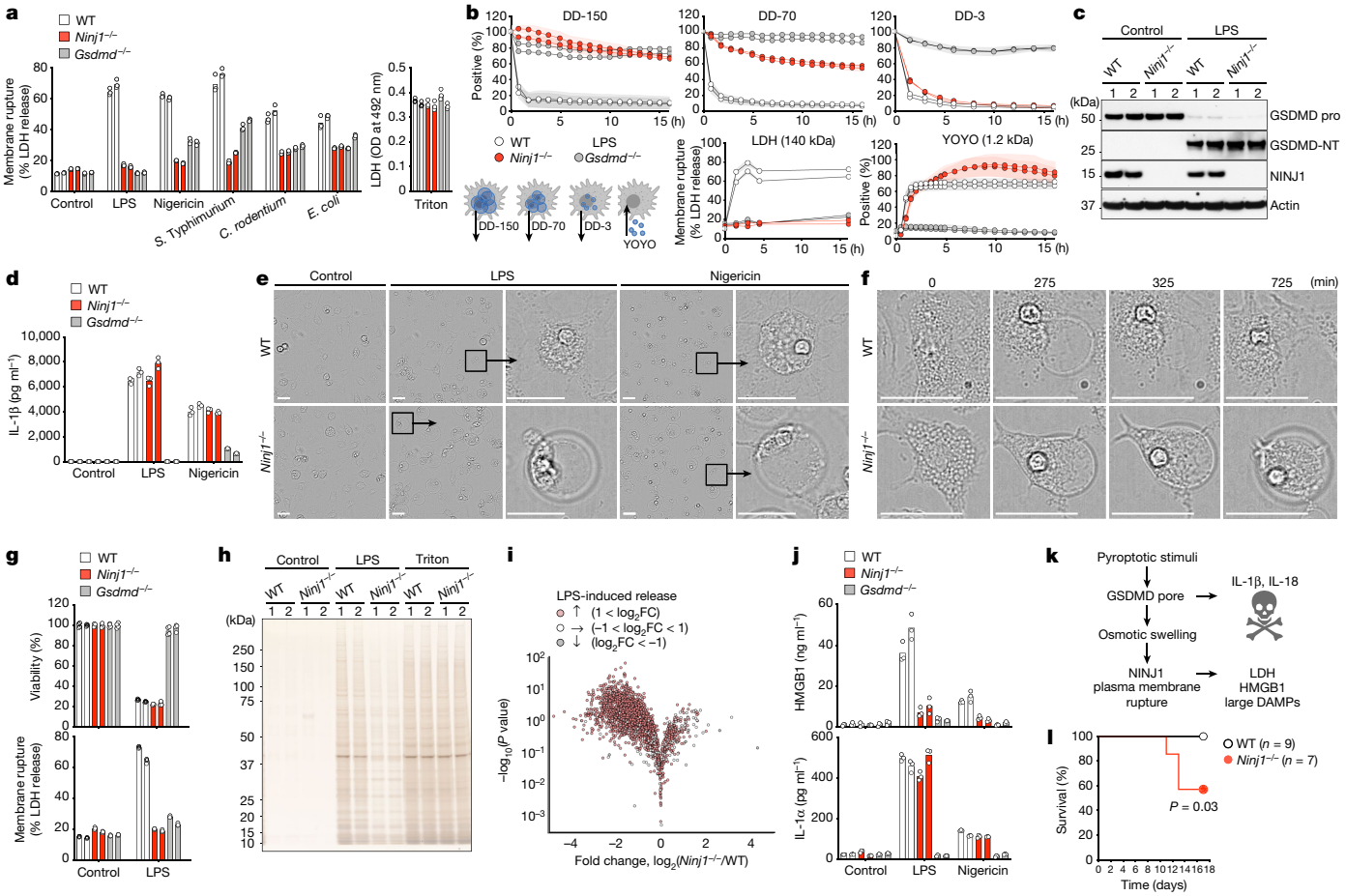

Fig. 2 | NINJ1 is essential for pyroptosis-related PMR. a, LDH released from primed BMDMs stimulated by LPS electroporation, nigericin or indicated bacteria, or treated with 0.25% Triton. **b**, Release of indicated kilodalton sizes of dextran dye (DD) or LDH, or incorporation of YOYO-1 in live-cell imaging analysis with primed BMDMs after LPS electroporation over a 16-h time course. Data are means (circles) ± s.d. (shaded area) of three individual replicates. **c**, Immunoblot of GSDMD, GSDMD-N-terminal fragment (GSDMD-NT) and NINJ1 in supernatant and extract from primed BMDMs after stimulation with LPS electroporation. NINJ1 is from a separate blot. **d**, Release of IL-1β from primed BMDMs stimulated with LPS electroporation or nigericin. **e**, Bright-field images of primed BMDMs stimulated with LPS transfection or nigericin for 16 h. **f**, Single-cell time course images of primed BMDMs after LPS transfection. **g**, Viability (top) or LDH release (bottom) of primed BMDMs at 16 h after LPS electroporation. **h**, **i**, Silver staining (**h**) or volcano plot (**i**) of released proteins in culture supernatant of primed BMDMs stimulated by LPS electroporation. FC, fold change. **j**, Release of HMGB1 or IL-1α from BMDMs stimulated as in **d**. **k**, Model for pyroptosis-related PMR. **l**, Kaplan–Meier survival plots for mice infected with *C. rodentium*. *P* value was calculated by a two-sided Gehan–Breslow–Wilcoxon test. Unless otherwise specified, data are means (bars) of at least three individual replicates (circles). $n = 2$ per genotype. Scale bars, 25 µm. For gel source data, see Supplementary Fig. 1.

LDH than wild-type BMDMs in response to necrotic stimuli (bacterial pore-forming toxins) or apoptotic stimuli (including chemotherapeutic agents such as the DNA crosslinker cisplatin and BCL-2 antagonist venetoclax)[22]. The release of HMGB1 and other proteins from BMDMs exposed to cisplatin or venetoclax was also attenuated by NINJ1 deficiency (Fig. 3b, Extended Data Fig. 3a). Wild-type BMDMs treated with venetoclax exhibited typical apoptotic morphology[1] including cell shrinkage and bleb formation. Blebbing was not prevented by *Ninj1* deficiency, but the dying cells developed a persistent ballooned morphology (Fig. 3c, d, Extended Data Fig. 3b, Supplementary Video 4). These data underscore a global role for NINJ1 in inducing PMR.

We confirmed that venetoclax-induced PMR in BMDMs was a gasdermin-independent, non-pyroptotic event. BMDMs express only *Gsdmd* and *Gsdme* (Extended Data Fig. 3c), but *Gsdmd*$^{-/-}$*Gsdme*$^{-/-}$ BMDMs exhibited normal PMR in response to venetoclax, releasing both DD-150 and LDH (Fig. 3e, f). Mitochondrial dysfunction that leads to depletion of ATP and consequent cell swelling[22,23] may be responsible for apoptosis-related PMR. Oligomycin (an inhibitor of ATP synthase) also induced gasdermin-independent but NINJ1-dependent PMR (Fig. 3f–h, Extended Data Fig. 3d, e).

NINJ1 is unlikely to be the only mediator of PMR because NINJ1 deficiency only partially attenuated the release of LDH and DD-150 from BMDMs undergoing MLKL-dependent necroptosis[24,25] after treatment with TNF plus the pan-caspase inhibitor zVAD (Fig. 3i, j). Overall protein release, including the release of HMGB1, was largely unaltered (Extended Data Fig. 3f, g). These data support the existence of a NINJ1-independent mechanism for PMR during necroptosis. It is possible that oligomerized MLKL[25] disrupts the plasma membrane to induce PMR directly, thereby bypassing the need for NINJ1.

NINJ1 oligomerizes to induce PMR

Ectopic expression of human or mouse NINJ1 in HEK293T cells caused marked cytotoxicity with concomitant release of LDH (Fig. 4a, Extended Data Fig. 4a–c). The *Drosophila* orthologues dNINJ-A and dNINJ-B were also cytotoxic, whereas dNINJ-C and NINJ2 were not (Fig. 4a, Extended Data Fig. 4a, c–e). Scanning mutagenesis identified a highly conserved, extracellular domain, which is predicted to be α-helical, as crucial for cell killing (Fig. 4b, Extended Data Fig. 4f–h). All NINJ1 mutants that contained five consecutive alanine substitutions within

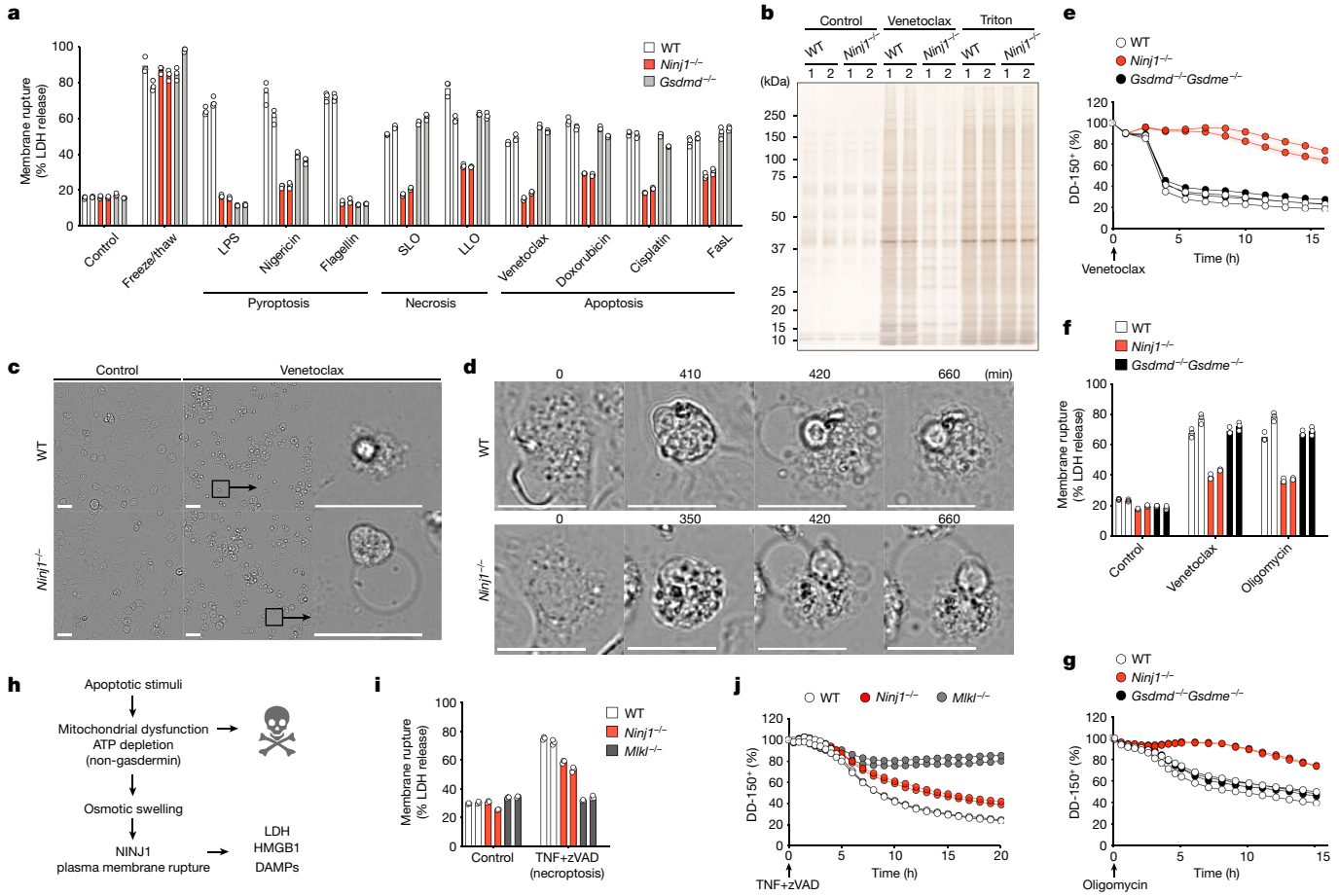

Fig. 3 | NINJ1 has a global role in PMR induction. a, LDH released from BMDMs after freeze/thaw cycle or culture with inducers of pyroptosis (LPS, nigericin and flagellin), necrosis (pore-forming toxins; listeriolysin O (LLO) and streptolysin O (SLO)), or apoptosis (venetoclax, doxorubicin, cisplatin and FasL). **b**, Silver stain of culture supernatant from BMDMs stimulated with venetoclax. **c**, Bright-field images of BMDMs cultured with venetoclax. **d**, Single-cell time-lapse images of BMDMs cultured with venetoclax. **e**, **g**, **j**, Release of DD-150 in BMDM live-cell imaging analysis after treatment with venetoclax (**e**), oligomycin (**g**), or TNF plus zVAD (**j**). Data are means (circles) ± s.d. (shaded area) of three individual replicates. **f**, **i**, LDH release from BMDMs stimulated with venetoclax and oligomycin (**f**), or TNF plus zVAD (**i**). **h**, Model for apoptosis-related PMR. Unless otherwise specified, data are means (bars) of at least three individual replicates (circles). $n = 2$ per genotype. Scale bars, 25 µm. For gel source data, see Supplementary Fig. 1.

the putative α-helical domain (including A42NKKS→A42AAAA) exhibited impaired cytotoxic activity. Mutating a residue within this region to a helix-breaking proline (including A59P), or amino acid replacements that mimic the NINJ2 sequence (S62M/Q63R), also reduced NINJ1 killing activity (Extended Data Figs. 4e, 5a, b). These results confirm the importance of this conserved, putative α-helix domain.

NINJ1 reportedly functions as a cell–cell adhesion molecule via homotypic binding of an adhesive segment (26–37 amino acids)[4,5] before the putative α-helix domain. However, mutagenesis of this evolutionarily variable segment did not reduce NINJ1 killing activity (Fig. 4b, Extended Data Fig. 4f). The previously reported adhesion-dead NINJ1(W29A) mutant[5] also restored LPS-induced PMR in *Ninj1*$^{-/-}$ iMACs (Extended Data Fig. 5c). Thus, the adhesive segment of NINJ1 appears dispensable for PMR.

We investigated NINJ1 activation in BMDMs using standard biochemical approaches. By SDS–PAGE, with or without reductant (dithiothreitol), NINJ1 migrated as an approximately 16-kDa monomer regardless of stimulus (LPS, nigericin, TLRs or interferons) or treatment with the pan-kinase inhibitor staurosporine (Extended Data Fig. 5d–f). By blue-native–PAGE (BN–PAGE), which maintains native protein structures, endogenous NINJ1 was shifted from approximately 40 to 900 kDa in response to nigericin or cytoplasmic LPS (Fig. 4c). These data suggest that NINJ1 exists as a dimer or trimer in unstimulated BMDMs, and then further oligomerizes in response to death stimuli.

By immunofluorescence microscopy of unstimulated BMDMs, NINJ1 primarily localized at the plasma membrane alongside the surface marker CD44, although some NINJ1, probably in transit, co-stained with the Golgi marker GM130 (Extended Data Fig. 6). After stimulation with nigericin, NINJ1 formed several speck-like assemblies (Fig. 4d), consistent with NINJ1 oligomerization.

The putative extracellular α-helix domain of NINJ1 possesses characteristic hydrophilic and hydrophobic clusters that are reminiscent of amphipathic α-helices[26,27] (Extended Data Fig. 7a). Of note, proteins that contain amphipathic helices such as α-synuclein and anti-microbial peptides (including Melittin bee venom) disrupt phospholipid bilayer membranes by an unknown mechanism in which positively charged residues have crucial roles[28,29]. Mutagenesis of positively charged NINJ1 residues (H40, K44, K45 and K65) to the non-charged amino acid glutamine uncovered a K45Q mutation that impaired NINJ1 cytotoxicity in HEK293T cells (Fig. 4e, Extended Data Fig. 7b). The K45 residue is evolutionarily conserved and predicted to be near the N-terminal side of the α-helix (Extended Data Figs. 4f, 7a). Both NINJ1(K45Q) and NINJ1(A59P) were unable to restore LPS-induced PMR in *Ninj1*$^{-/-}$ iMACs, and attenuated oligomerization of NINJ1 (Fig. 4f, g). These data support a model in which NINJ1 oligomerizes to induce PMR. A peptide corresponding to the putative α-helix domain of NINJ1 directly damaged synthetic liposome membranes to release encapsulated cargo (Extended Data Fig. 7c). Precisely how NINJ1 induces

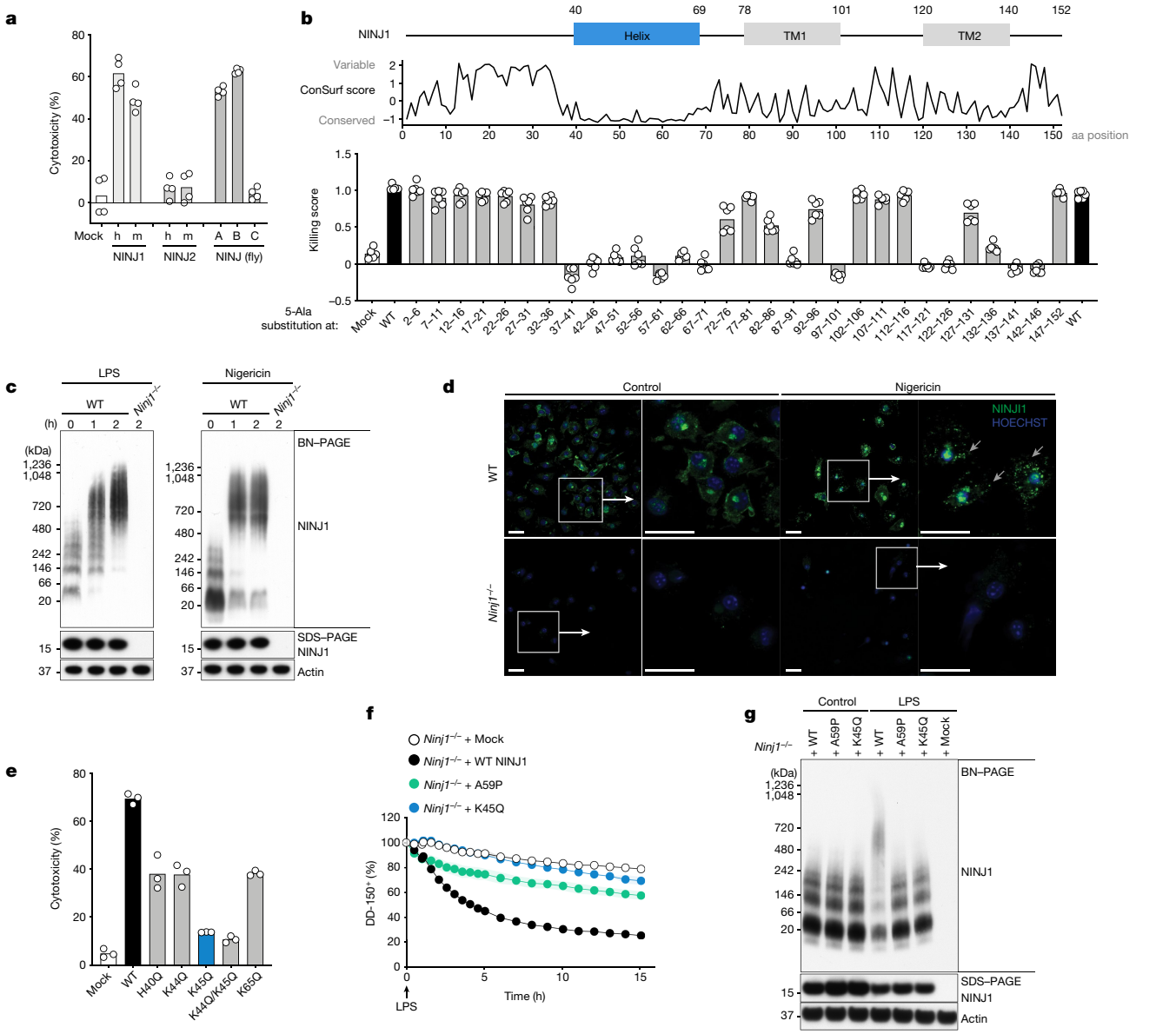

Fig. 4 | NINJ1 oligomerizes for induction of PMR. a, Cytotoxicity of Flag-tagged human (h) and mouse (m) NINJ1, NINJ2, and fly NINJ (dNINJ-A, -B, -C) in HEK293T cells. Data are means (bars) of at least four individual replicates (circles). **b**, Top, NINJ1 domain structure. Middle, conservation of NINJ1 amino acid (aa) residues as scored by ConSurf profile. Bottom, cytotoxicity of wild-type and 5-Ala scan NINJ1 mutants in HEK293T cells. Numbers indicate amino acid positions replaced by 5-Ala. Killing score is the cytotoxicity normalized against wild-type NINJ1 control. Data are means (bars) of at least six individual replicates (circles). **c**, BN–PAGE analysis of endogenous NINJ1 in primed BMDMs after LPS or nigericin stimulation for indicated periods. **d**, Immunofluorescence microscopy of NINJ1 in nigericin-stimulated primed BMDMs. Grey arrows highlight representative NINJ1 specks. Scale bars, 25 µm. **e**, Cytotoxicity of Flag-tagged NINJ1 mutants in HEK293T cells. Data are means (bars) of at least three individual replicates (circles). **f**, DD-150 dye release from *Ninj1*$^{-/-}$ iMACs reconstituted with NINJ1 after LPS electroporation. Data are means (circles) ± s.d. (shaded area) of three individual replicates. **g**, BN–PAGE analysis of reconstituted NINJ1 in LPS electroporation-stimulated iMACs. Results in **c** and **g** represent two independent experiments. For gel source data, see Supplementary Fig. 1.

PMR remains unclear and will probably require further structural insights. Given that NINJ1 mediates PMR during pyroptosis, necrosis and apoptosis (Fig. 3a), a common event such as an increase in cell volume may trigger activation of NINJ1. Some amphipathic helices sense lipid-packing defects and altered membrane curvature[26,30], both of which may be caused by cell swelling. Although NINJ1 appears to be required for end-stage lysis, its mechanism of action remains undefined. The link between PMR and NINJ1 may well be indirect and not specific to programmed PMR.

In summary, NINJ1 is an evolutionarily conserved cell-surface protein that mediates PMR and the release of DAMPs—key events in the propagation of inflammation. Given the potent and global role for NINJ1 in PMR induction and DAMP-release related to pyroptosis, apoptosis and necrosis, targeting NINJ1 may be of therapeutic benefit. Indeed, the addition of a monoclonal NINJ1 antibody to cell cultures expressing endogenous NINJ1 inhibited PMR (Extended Data Fig. 7d).

Online content

Any methods, additional references, Nature Research reporting summaries, source data, extended data, supplementary information, acknowledgements, peer review information; details of author contributions and competing interests; and statements of data and code availability are available at https://doi.org/10.1038/s41586-021-03218-7.

1. Fink, S. L. & Cookson, B. T. Apoptosis, pyroptosis, and necrosis: mechanistic description of dead and dying eukaryotic cells. *Infect. Immun*. **73**, 1907–1916 (2005).
2. Gaidt, M. M. & Hornung, V. Pore formation by GSDMD is the effector mechanism of pyroptosis. *EMBO J*. **35**, 2167–2169 (2016).
3. Kayagaki, N. & Dixit, V. M. Rescue from a fiery death: a therapeutic endeavor. *Science* **366**, 688–689 (2019).
4. Araki, T. & Milbrandt, J. Ninjurin, a novel adhesion molecule, is induced by nerve injury and promotes axonal growth. *Neuron* **17**, 353–361 (1996).
5. Araki, T., Zimonjic, D. B., Popescu, N. C. & Milbrandt, J. Mechanism of homophilic binding mediated by ninjurin, a novel widely expressed adhesion molecule. *J. Biol. Chem*. **272**, 21373–21380 (1997).
6. Ahn, B. J. et al. The N-terminal ectodomain of Ninjurin1 liberated by MMP9 has chemotactic activity. *Biochem. Biophys. Res. Commun*. **428**, 438–444 (2012).
7. Lee, H. J. et al. Ninjurin1 mediates macrophage-induced programmed cell death during early ocular development. *Cell Death Differ*. **16**, 1395–1407 (2009).
8. Yang, H. J. et al. Ninjurin 1 has two opposing functions in tumorigenesis in a p53-dependent manner. *Proc. Natl Acad. Sci. USA* **114**, 11500–11505 (2017).
9. Cookson, B. T. & Brennan, M. A. Pro-inflammatory programmed cell death. *Trends Microbiol*. **9**, 113–114 (2001).
10. Shi, J. et al. Cleavage of GSDMD by inflammatory caspases determines pyroptotic cell death. *Nature* **526**, 660–665 (2015).
11. Kayagaki, N. et al. Caspase-11 cleaves gasdermin D for non-canonical inflammasome signalling. *Nature* **526**, 666–671 (2015).
12. Ding, J. et al. Pore-forming activity and structural autoinhibition of the gasdermin family. *Nature* **535**, 111–116 (2016).
13. Liu, X. et al. Inflammasome-activated gasdermin D causes pyroptosis by forming membrane pores. *Nature* **535**, 153–158 (2016).
14. Fink, S. L. & Cookson, B. T. Caspase-1-dependent pore formation during pyroptosis leads to osmotic lysis of infected host macrophages. *Cell. Microbiol*. **8**, 1812–1825 (2006).
15. Ruan, J., Xia, S., Liu, X., Lieberman, J. & Wu, H. Cryo-EM structure of the gasdermin A3 membrane pore. *Nature* **557**, 62–67 (2018).
16. Kayagaki, N. et al. Non-canonical inflammasome activation targets caspase-11. *Nature* **479**, 117–121 (2011).
17. de Vasconcelos, N. M., Van Opdenbosch, N., Van Gorp, H., Parthoens, E. & Lamkanfi, M. Single-cell analysis of pyroptosis dynamics reveals conserved GSDMD-mediated subcellular events that precede plasma membrane rupture. *Cell Death Differ*. **26**, 146–161 (2019).
18. DiPeso, L., Ji, D. X., Vance, R. E. & Price, J. V. Cell death and cell lysis are separable events during pyroptosis. *Cell Death Discov*. **3**, 17070 (2017).
19. Andersson, U. & Tracey, K. J. HMGB1 is a therapeutic target for sterile inflammation and infection. *Annu. Rev. Immunol*. **29**, 139–162 (2011).
20. Štros, M. HMGB proteins: interactions with DNA and chromatin. *Biochim. Biophys. Acta* **1799**, 101–113 (2010).
21. Silva, M. T. Secondary necrosis: the natural outcome of the complete apoptotic program. *FEBS Lett*. **584**, 4491–4499 (2010).
22. Ashkenazi, A., Fairbrother, W. J., Leverson, J. D. & Souers, A. J. From basic apoptosis discoveries to advanced selective BCL-2 family inhibitors. *Nat. Rev. Drug Discov*. **16**, 273–284 (2017).
23. Dijkstra, K., Hofmeijer, J., van Gils, S. A. & van Putten, M. J. A biophysical model for cytotoxic cell swelling. *J. Neurosci*. **36**, 11881–11890 (2016).
24. Sun, L. et al. Mixed lineage kinase domain-like protein mediates necrosis signaling downstream of RIP3 kinase. *Cell* **148**, 213–227 (2012).
25. Grootjans, S., Vanden Berghe, T. & Vandenabeele, P. Initiation and execution mechanisms of necroptosis: an overview. *Cell Death Differ*. **24**, 1184–1195 (2017).
26. Drin, G. & Antonny, B. Amphipathic helices and membrane curvature. *FEBS Lett*. **584**, 1840–1847 (2010).
27. Peter, B. J. et al. BAR domains as sensors of membrane curvature: the amphiphysin BAR structure. *Science* **303**, 495–499 (2004).
28. Auluck, P. K., Caraveo, G. & Lindquist, S. α-Synuclein: membrane interactions and toxicity in Parkinson's disease. *Annu. Rev. Cell Dev. Biol*. **26**, 211–233 (2010).
29. Zasloff, M. Antimicrobial peptides of multicellular organisms. *Nature* **415**, 389–395 (2002).
30. Hatzakis, N. S. et al. How curved membranes recruit amphipathic helices and protein anchoring motifs. *Nat. Chem. Biol*. **5**, 835–841 (2009).

Methods

ENU-mutagenized mouse strains

C57BL/6NCrl G0 mice were treated with ENU and the resulting mutations were bred to homozygosity in G3 mice as previously described[31]. All mice used in this study were cared for and used in experiments approved by the Australian National University Animal Experimentation Ethics Committee under protocol A2018/07. 129X1/SvJ strain was used as a *Casp11* mutant[16] control.

Exome sequencing

Exon capture, sequencing and analysis were performed as previously described[32,33]. *Ninj1* mutant genotyping primer sequences: F1: GAAGGTGACCAAGTTCATGCTCTGACCGCCTTGCTCCCACA; F2: GAAGGTCGGAGTCAACGGATTCTGACCGCCTTGCTCCCACT; R1: CGCTCTTCTTGTTGGCATAA.

Other mice

Gsdmd$^{-/-}$ (1,632-bp deletion[11]) mice, *Casp11*$^{-/-}$ mice[16] and *Mlkl*$^{-/-}$mice[34] with C57BL/6N background were previously described. *Gsdme*$^{-/-}$ (2-bp deletion at exon 3) mice with C57BL/6N background were genotyped with PCR primers (5′-TACCTCTTGACGGCATCC and 5′- ATACGAGAGCAAGTGTGAGA) yielding a 171-bp wild-type DNA fragment and a 169-bp mutant DNA fragment, and crossed with *Gsdmd*$^{-/-}$ mice to generate *Gsdmd*$^{-/-}$*Gsdme*$^{-/-}$ mice (Extended Data Fig. 8a). *Ninj1*$^{-/-}$ mice were obtained by electroporation-based strategy of C57BL/6N zygotes with 25 ng μl^{-1} wild-type *Cas9* mRNA (Thermo Fisher Scientific) and 13 ng μl^{-1} in vitro-transcribed two single-guide RNAs into mouse zygotes[35]. Tail DNA from resulting offspring was analysed by PCR and sequencing. Target sequences of sgRNA used to knockout exon 2 are: 5′-AAGGTGACCAACGTCCTGTA-3′ PAM: GGG with an CFD algorithm score of 97, and the 5′-CCATACGCCTTACTCCCTGA-3′PAM:GGG with an CFD algorithm score of 94. The 867-bp knockout region corresponds to GRCm38/mm10 chr13: 49,193,197–49,194,063. *Ninj1*$^{-/-}$ mice were genotyped with PCR primers (FAM 5′-CAGGTTGGTGGTACATCTATTG, 5′-GCAGCAGGTACTTCTCC, and 5′-ACGGACGACCAGTGATTA) yielding a 358-bp wild-type DNA fragment and a 408-bp mutant DNA fragment. For wild-type control, *Ninj1*$^{+/+}$ littermate mice were used. All animal procedures were conducted under protocols approved by the Genentech Institutional Animal Care and Use Committee in an Association for Assessment and Accreditation of Laboratory Animal Care (AAALAC)-accredited facility in accordance with the Guide for the Care and Use of Laboratory Animals and applicable laws and regulations. Groups were determined by genotype rather than treatment, therefore, randomization was not applicable. Mice were picked and treated by the same individual, therefore, blinding to genotype and treatment as well as during data collection and analysis was not possible. No statistical methods were used to predetermine sample size.

Reagents and antibodies

Ultra-pure LPS (*E. coli* O111:B4, InvivoGen), Pam3CSK4 (InvivoGen), IFNα (PBL Assay Science), IFNγ (eBioscience), nigericin (MilliporeSigma), Ultra-pure flagellin (from *P. aeruginosa*, InvivoGen), cholera toxin B (CTB, List Biological Labs), venetoclax (TOCRIS), doxorubicin (Enzo Life Sciences), cisplatin (Fresenius Kabi), oligomycin A (TOCRIS), staurosporine (Enzo Life Sciences), TNF (in-house Genentech), carbobenzoxy-valyl-alanyl-aspartyl-[O-methyl]-fluoromethylketone (z-VAD-FMK, Promega), listeriolysin-O (LLO, US Biologicals), streptolysin-O (SLO, US Biologicals) and FasL (MegaFasL, AdipoGen). Antibodies used include: GSDMD (clone 17G2G9[36], Genentech, 0.2 μg ml^{-1}), GSDMD-NT (cleaved GSDMD Asp276, 50928S, Cell Signaling Technology, 1 μg ml^{-1}), GSDME polyclonal antibody (raised against mouse GSDME E74–G93 peptide, rabbit IgG, Genentech, 0.5 μg ml^{-1}; Extended Data Fig. 8a), S6 ribosomal protein (5G10, Cell Signaling Technology, 1 μg ml^{-1}), phospho-S6 (D57.2.2E, Cell Signaling Technology, 1 μg ml^{-1}), β-actin HRP (AC-15, Novus Biologicals, 0.1 μg ml^{-1}), Flag epitope (M2 HRP, MilliporeSigma, 1 μg ml^{-1}), HRP-anti-rat (Jackson Immunoresearch, 112-035-175, 1:5,000 dilution), HRP-anti-rabbit (Jackson Immunoresearch, 111-035-047 and 111-035-046, 1:5,000 dilution), and anti-mouse NINJ1 monoclonal antibody (raised against mouse NINJ1 extracellular domain 1, epitope P22–L31, rabbit IgG2b, clone 25, Genentech, 0.2 μg ml^{-1}; Extended Data Fig. 8b). Where indicated, anti-mouse NINJ1 polyclonal antibody 312 (raised against mouse NINJ1 extracellular domain 1, rabbit IgG, Genentech, 1 μg ml^{-1}) and anti-human NINJ1 (NBP1-59210, Novus Biologicals, 1 μg ml^{-1}) were used.

BMDM stimulation

Bone marrow cells were differentiated into macrophages in DMEM supplemented with 10% (v/v) low-endotoxin fetal bovine serum (FBS; Omega Scientific) and 20% (v/v) L929-conditioned medium at 37 °C with 5% CO_2 and were collected on day 5 for experiments. For stimulation, cells were plated overnight at approximately 1.0×10^6 cells ml^{-1} in 100 μl on 96-well plates or in 500 μl for 24-well plates. For 96-well-based inflammasome stimulations, cells were primed with Pam3CSK4 (1 μg ml^{-1}) for 5 h where indicated, which was followed by stimulation with 10 μg ml^{-1} nigericin, or LPS (described as follows) in Opti-MEM I media (Thermo Fisher Scientific). For intracellular LPS electroporation[37], primed BMDMs were electroporated with the 4D-Nucleofector Y Unit (Lonza) in Opti-MEM I medium with LPS (5 μg ml^{-1}) in 24-well plates. Unless indicated, after 1 h nigericin or 2 h LPS electroporation, cells and culture supernatant were subjected to analysis. For flagellin stimulation, primed BMDMs were electroporated with flagellin (0.5 μg ml^{-1}) with 4D-Nucleofector Y Unit and cultured for 0.5 h. For bacterial infections with *E. coli* (ATCC 11775, MOI 30), *C. rodentium* (ATCC 51116, MOI 20) and *S.* Typhimurium (SL1344, MOI 10), primed BMDMs were cultured with bacteria for 1.5 h and then gentamicin (Thermo Fisher Scientific) was added to cultures at 100 μg ml^{-1}, which was followed by additional incubation for a total 16 h. For FasL (0.5 μg ml^{-1} for 6 h), oligomycin (12.6 μM for 16 h), venetoclax (25 μM for 16 h), doxorubicin (10 μM for 16 h), cisplatin (10 μg ml^{-1} for 16 h), LLO (2 μg ml^{-1} for 6 h), SLO (1 μg ml^{-1} for 6 h), TNF plus zVAD (TNF 100 ng ml^{-1} plus z-VAD-FMK 20 μM for 16 h), non-primed BMDMs were used. For triton lysis controls, cells were lysed with 0.25% triton-X in corresponding medium. For freeze and thaw, cells were frozen at −80 °C for 30 min in 96-well plates, then thawed at room temperature. For TLR or interferon stimulation, BMDMs were cultured with Pam3CSK4 (1 μg ml^{-1}), LPS (1 μg ml^{-1}), IFNα (100 ng ml^{-1}) and IFNγ (100 ng ml^{-1}) and stimulated for 6 h. For staurosporine treatment, primed BMDM were pre-cultured with 1 μM staurosporine for 30 min before LPS or nigericin stimulation.

Cell assays and cytokine measurements

Culture medium was analysed for LDH release with the CytoTox 96 Non-Radioactive Cytotoxicity Assay (Promega) and for IL-1β secretion with the mouse IL-1β Tissue Culture Kit (Meso Scale Discovery). Enzyme-linked immunosorbent assay (ELISA) kits were used to assay IL-18 (MBL International), IL-1α (Thermo Fisher Scientific), and HMGB1 (IBL). For IL-6 and TNF, Luminex analysis was run with Milliplex Mouse Panel I 32-plex (MilliporeSigma). CellTiter-Glo reagent (Promega) was used for ATP assay for detection of viable cells. For YOYO-1 staining, medium containing YOYO-1 (491/509) dye (Thermo Fisher Scientific) at a final concentration of 200 nM was added at the time of stimulation. Images were scanned in the green channel every hour for at least 16 h with IncuCyte S3 (Essen BioScience) at 10 × magnification. Nuclear-ID Red DNA stain (Enzo Life Sciences) was added after the last time point and scanned in the red channel. IncuCyte software was used to determine the total number of YOYO$^+$ cells and Nuclear-ID$^+$ cells (total cells). The percentage of YOYO$^+$ cells was calculated as the number of YOYO$^+$ cells divided by the total number of Nuclear-ID$^+$ cells. Plots were generated using Prism (GraphPad).

Dextran dye release assay

BMDM stimulation was carried out as described above with the following modifications. Before plating, BMDMs were loaded with dextran dye conjugates (fluorescein isothiocyanate-dextran, 150 kDa, MilliporeSigma; Texas Red-dextran, 70 kDa, 3 kDa, Thermo Fisher Scientific) using a 100 µl neon tip (Thermo Fisher Scientific). Approximately 5.0×10^6 BMDMs were electroporated in 120 µl R buffer (Thermo Fisher Scientific) with 12 µl of dextran dye at 50 mg ml^{-1}. Before plating, BMDMs were washed with high-glucose DMEM. After stimulation, images of BMDMs were scanned over 16 h with IncuCyte S3 (Essen BioScience) at 10× magnification. Plots were generated using Prism.

Sample preparation for immunoblot

For standard immunoblot (extract only), 1.0×10^5 cells were lysed by incubation with (15–75) µl lysis buffer (10 mM Tris pH7.5, 150 mM NaCl, 1% NP-40, 2.5 mM $MgCl_2$, 0.5 mM $CaCl_2$, 5 µg ml^{-1} DNase (Qiagen), 1 × Complete Protease Inhibitor (Roche Applied Science) and PhosSTOP phosphatase inhibitor (MilliporeSigma)) at 4 °C for 30 min. The lysate was mixed with NuPAGE LDS sample buffer 4× (Thermo Fisher Scientific) and run as whole cell lysate in SDS–PAGE or Phos-tag SDS–PAGE (FUJIFILM). For preparation of supernatant and extract, 1.0×10^6 primed BMDMs were electroporated with 1.0 µg LPS in 100 µl R buffer using neon 100 µl tip with 1,720 voltage, 10 width, 2 pulse settings. Electroporated cells were added to 60 µl Opti-MEM I medium to make a total of 70 µl. For nigericin stimulation, 1.0×10^6 primed BMDMs were suspended with 10 µg ml^{-1} nigericin in 70 µl Opti-MEM I medium. Cells were incubated for 2 h. Samples were collected by pelleting cells and transferring supernatant to a separate tube with 1 × Complete Protease Inhibitor added to supernatant. Remaining cells were lysed in 40 µl of lysis buffer and 37 µl of LDS sample buffer 4×. Cell extracts were then combined with supernatant for immunoblotting.

RNA-sequencing

Total RNA was extracted from primed or non-primed wild-type BMDMs and *Ninj1*$^{-/-}$ BMDMs ($n = 3$ per genotype) using an RNeasy kit (Qiagen) with on-column DNase digestion. Quality control of total RNA was performed to determine sample quantity and quality. The concentration of RNA was determined using a NanoDrop 8000 (Thermo Fisher Scientific), and the integrity of the RNA was determined by Fragment Analyzer (Advanced Analytical Technologies). Total RNA (100 ng) was used as an input material for library preparation using the TruSeq Stranded Total RNA Library Prep Kit (Illumina). The sizes of the libraries were confirmed using High Sensitivity D1K screen tape (Agilent Technologies), and their concentrations were determined with a quantitative PCR–based method using a Library Quantification kit (KAPA). The libraries were multiplexed and sequenced on an Illumina HiSeq4000 (Illumina) to generate 30 million single-end, 50 bp reads. For RNA-seq analysis, the raw FASTQ reads were aligned to the mouse reference genome (GRCm38-mm10) using GSNAP (with parameters -M 2 -n 10 -B 2 -i 1 -N 1 -w 200000 -E 1 --pairmax-rna = 200000 --clip-overlap). Reads were filtered to include only the uniquely mapped reads. Differential expression analysis was performed using the voom/limma R package. Genes were considered to be differentially expressed if the $\log_2$-transformed fold change was > 1 or < −1 and the adjusted P value was < 0.05.

Lipidomics analysis

Approximately 5.0×10^6 primed BMDMs pellets were suspended in PBS and lysed using an ultrasound sonicator. Then, 750 µl water, 0.9 ml dichloromethane (DCM, Honeywell Burdick & Jackson, >99.5%) and 2 ml methanol (HPLC grade, Fisher Chemical) were added to 250 µl of cell lysate (2.5×10^6 cells) to form a single phase. After a 30-min incubation, isotopically labelled internal lipid standards (Lipidyzer, SCIEX) were added to the mixture, followed by 0.9 ml DCM and 1 ml water. The mixture was vortexed and centrifuged at 1,000g for 10 min to achieve phase separation. The bottom layer was collected into a clean glass tube, and the upper layer was extracted once more by adding 1.8 ml of DCM. The bottom layer of the second extraction was combined with the first and dried under a gentle stream of nitrogen for subsequent LC–MS/MS analysis. Dried residue was reconstituted in 300 µl DCM:methanol (1:1), 10 mM ammonium acetate for direct infusion and analysis on a SelexION enabled 6500+ QTRAP mass spectrometry (SCIEX) by the method previously described[38]. For cholesterol analysis, dried residue was reconstituted in 200 µl DCM: methanol (1:1). HPLC separation of cholesterol from its metabolites was performed on a reverse-phase column (Luna Omega 1.6 µm C18 100A, LC column 100 × 2.1 mm). The temperatures of the column oven and auto sampler were set at 40 °C and 15 °C, respectively. The LC flow rate was set at 0.2 ml min^{-1}. Initial gradient conditions were 95% mobile phase A (3:1 water: methanol) and 5% mobile phase B (1:1 methanol: isopropanol). Mobile phase B was increased to 55% within 2 min, further increased to 65% over 12 min and then to 74% in 7 min. Mobile B was held at 74% for 11 min and increased to 100% in 4 min. Mobile phase B was returned to the initial conditions within 1 min and re-equilibrated for 5 min before the next injection. The liquid chromatograph was coupled to a 6500+ QTRAP mass spectrometer operated under positive ionization mode with the following source settings: turbo-ion-spray source at 500 °C, N_2 nebulization at 20 psi, N_2 heater gas at 20 psi, curtain gas at 30 psi, collision-activated dissociation gas pressure was held at medium, turbo ion-spray voltage at 5500 V, declustering potential at 60 V, entrance potential at 10 V and collision energy of 30 V. Sample analysis was performed in multiple reactions monitoring mode with a dwell time of 0.10 s. The transitions monitored for cholesterol and D7-cholesterol were 369.4/161 and 376.3/161, respectively. Cholesterol quantification was achieved by creating a standard curve using six concentration levels of cholesterol versus its normalized response to the internal standard (D7-cholesterol). Plots were generated using Prism.

Secretome analysis of BMDM supernatants

Approximately 5.0×10^6 primed BMDMs were neon-electroporated with 5 µg of LPS with 1,720 voltage, 10 width, 2 pulse settings. BMDMs were incubated in 250 µl of no-FBS high-glucose DMEM for 2 h, then pelleted by spinning at 300g for 10 min. Then, 20 µl of supernatants from two replicates of wild-type or *Ninj1*$^{-/-}$ BMDMs were reduced with 10 mM dithiothreitol at 60 °C followed by alkylation with 20 mM iodoacetamide at room temperature. Proteins were digested with 0.2 µg trypsin (Promega) in ammonium bicarbonate pH 8.0 at 37 °C overnight. Digestion was quenched with formic acid and the supernatants were subjected to desalting on C18 PhyTips (PhyNexus), lyophilized, reconstituted to 25 µl in 0.1% formic acid containing 2% acetonitrile and analysed without further processing by reversed phase nano-LC–MS/MS on a Waters NanoAcquity HPLC system (Waters) interfaced to a Thermo Fisher Fusion Lumos (Thermo Fisher Scientific). Peptides were loaded onto a Symmetry C18 column (1.7 mm BEH-130, 0.1 × 100 mm, Waters) and separated with a 60 min gradient from 2% to 25% solvent B (0.1% formic acid, 98% acetonitrile) at 1 µl min^{-1} flow rate. Peptides were eluted directly into the mass spectrometer with a spray voltage of 1.2 kV. Full MS data were acquired in FT for 350–1,250 m/z with a 60,000 resolution. The most abundant ions found from full MS were selected for MS/MS through a 2-Da isolation window. Acquired tandem MS spectra were searched using the Mascot (Matrix Sciences) with trypsin enzyme specificity. Search criteria included a full MS tolerance of 50 ppm, MS/MS tolerance of 0.5 Da with oxidation (+15.9949 Da) of as variable modification and carbamidomethylation (+57.0215 Da) of cysteine as static modification. Data were searched against the mouse and contaminant subset of the Uniprot database that consists of the reverse protein sequences. Peptide assignments were first filtered to a 2% false discovery rate (FDR) at the peptide level and subsequently to a 2% FDR at the protein level. Label free quantification was performed

using the Vista Algorithm[39] and peptide spectral matches (PSMs) per protein were visualized using Spotfire (TIBCO). Top hits were identified by multiplying the $\log_2$-transformed fold change (fold change comparing *Ninj1*$^{-/-}$ to wild-type BMDMs) by the $\log_{10}P$ value.

Silver staining of total proteins in culture supernatant

For visualization of secreted proteins, primed BMDMs were washed with PBS three times and cultured in no-FBS high-glucose DMEM medium for 4 h after LPS electroporation or nigericin stimulation. Culture supernatant was collected after spinning for 10 min at 300*g*. Then, 10 µl of the supernatant was run on SDS–PAGE and proteins were silver stained by using SilverQuest (Thermo Fisher Scientific). For venetoclax and TNF plus zVAD stimulation, non-primed BMDMs were cultured with venetoclax or TNF plus zVAD for 16 h.

Plasmids and transient expression

cDNAs encoding N-terminal Flag- or non-tagged (human and mouse) NINJ1, NINJ2, *D. melanogaster* NINJ-A, -B, -C, N-terminal Flag-tagged mouse NINJ1 5-Ala-scanning mutants, N-terminal Flag-tagged mouse NINJ1 single Pro mutants, N-terminal Flag-tagged mouse NINJ1 mutants (H, K/Q SQ/MR mutants), and N-terminal GST–Flag-tagged mouse NINJ1 epitope (P22–L31) were synthesized and subcloned into pcDNA3.1/Zeo(+) (Thermo Fisher Scientific). For transient expression in HEK293T cells (ATCC, tested for mycoplasma contamination but not authenticated), 2.6×10^4 cells were reverse transfected with 50 ng of plasmid with 0.16 µl Lipofectamine 2000 (Thermo Fisher Scientific) per well in 96-well plates. At 16 h after transfection, cytotoxicity was measured by CellTiter-Glo reagent.

Generation of stable cell lines

ER-Hoxb8-immortalized, wild-type and *Ninj1*$^{-/-}$ C57BL6/N mice-derived iMACs were made as previously reported[40], and maintained in RPMI 1640 medium supplemented with 10% (v/v) low-endotoxin FBS, murine granulocyte-macrophage colony-stimulating factor (GM-CSF, 20 ng ml^{-1}, eBioscience), and 1 µM β-oestradiol (MilliporeSigma). For reconstitution of *Ninj1*, cDNAs encoding non-tagged mouse NINJ1 or mutants (W29A, A59P, K45Q) were synthesized and subcloned into the piggyBac vector (BH1.11, Genentech). *Ninj1*$^{-/-}$ iMACs were co-electroporated with NINJ1/BH1.11 and a transposase vector (pBO, Transposagen Biopharmaceuticals) using neon electroporation. Cells were selected with 6.25 µg ml^{-1} blasticidin (Thermo Fisher Scientific). LPS neon electroporation and dextran dye release were performed as described for BMDMs above.

BN–PAGE

BMDMs or iMACs were lysed with native-PAGE lysis buffer (1% Digitonin (Thermo Fisher Scientific), 50 mM Tris pH7.5, 150 mM NaCl, 1 × Complete Protease Inhibitor). After centrifuging at 20,800*g* for 30 min, lysates were mixed with NativePAGE sample buffer 4× (Thermo Fisher Scientific) and subjected to BN–PAGE[41] using NativePAGE 3–12% Gel (Thermo Fisher Scientific) and Coomassie G-250 (Thermo Fisher Scientific).

Immunofluorescence

BMDMs were stimulated with nigericin on glass-bottom SensoPlates (Greiner). Cells were fixed with 4% paraformaldehyde in PBS and permeabilized with 0.1% Tween-20. Plates were blocked in PBS supplemented with 10% goat serum and 0.1% Tween-20 for 1 h at room temperature. Next, cells were incubated with primary antibody at 4 °C overnight, followed by Alexa Fluor 488 or Alexa Fluor 647 secondary (Thermo Fisher Scientific, diluted 1:500) at room temperature for 1 h. Nuclei were stained with 0.5 µg ml^{-1} HOECHST dye (Thermo Fisher Scientific) for 10 min at room temperature. Primary antibodies used include: TOMM20 (clone 2F8.1, MilliporeSigma, diluted 1:100), CD44 (KM201, Abcam, diluted 1:500), and GM130 (clone 35, BD Biosciences, diluted 1:100). Plates were imaged using a 60× Plan Fluor objective on an ImageXpress Micro Confocal system (Molecular Devices) using MetaXpress (Molecular Devices). Images were subsequently processed using the scikit-image python package.

Live imaging of BMDMs

BMDMs were plated on glass-bottom SensoPlates. For LPS transfection on the glass-bottom plate, primed BMDMs were cultivated with 5 µg ml^{-1} LPS and 20 µg ml^{-1} CTB to deliver LPS inside place[37]. Where described, tetramethylrhodamine methyl ester perchlorate (TMRM, 200 µM, Thermo Fisher Scientific), HOECHST, and DD-150 were used. Plates were imaged either using a 60× Plan Fluor or 20× Super Plan Fluor ELWD objective on an ImageXpress Micro Confocal system equipped with an environmental controller and gas mixer to maintain cells at 37 °C and 5% CO_2. Images of the bright-field and transmitted light and fluorescence channels were imaged every 5 min overnight. Images were subsequently processed and videos were generated using the scikit-image python package.

Lattice light-sheet microscopy

BMDMs were plated on 5 mm round coverslips in 6 well plates. Primed BMDMs were incubated with CellMask Deep Red Plasma membrane Stain (5 µg ml^{-1} Thermo Fisher Scientific) for 20 min. 4D datasets were generated using a lattice light-sheet microscope (Intelligent-Imaging Innovations). Coverslips were mounted to sample holders and placed in a 2.5 ml bath containing phenol red free DMEM (Thermo Fisher Scientific) with 160 µg ml^{-1} nigericin to stimulate bubble formation. A lattice light-sheet used for illumination was generated using a 640 nm laser and a 0.450 NAO/0.375 NAI annular mask. Entire cell volume was imaged using Z galvo sweep of the light sheet through the sample and a Flash 4 sCMOS camera (Hamamatsu). A total of 201 *Z* planes at 0.2-µm steps (0.1 post deskew), 10 ms exposure time and 5% laser power. Images were acquired and deskewed with Slidebook 6 (Intelligent-Imaging Innovations). Time-lapse images were imported into Imaris 9.5 (Oxford Instruments) to generate time-lapse videos for presentation.

Secondary structure prediction and helix modelling

Secondary structure prediction for mouse NINJ1 was performed using the JPred 4 server. Following prediction, the external alpha helical domain was modelled with SWISS-MODEL[42] and subsequently visualized with PyMOL (v.2.3.5). The structure was exported using ray-traced frames.

Conservation scores, sequence alignments, and phylogenetic tree generation

The conservation score for each amino acid residue of NINJ1 was calculated using the ConSurf[43,44] server and plotted using the Matplotlib python package. Individual orthologue NINJ1 and NINJ2 sequences obtained from the UniProt database[45] were aligned using the Clustal Omega multiple sequence alignment[46]. Phylogenetic trees were retrieved from the resulting Clustal Omega output and the alignment was visualized using ESPript 3.0[47].

Circular dichroism spectroscopy

Secondary structures of the synthesized human NINJ1 α-helix region peptide (HYASKKSAAESMLDIALLMANASQLKAVVE) was measured on a JASCO J-815 spectropolarimeter (JASCO) equipped with a thermostable cell holder equilibrated to 20 °C. Peptide solutions (from 10 mg ml^{-1} stocks in 5% DMSO in ddH_2O) were prepared in sodium phosphate buffer (20 mM sodium phosphate (pH 7.47, 2.0 N NaOH), 10 mM NaCl, 1% sodium dodecyl sulfate). Final peptide concentrations were determined by Pierce BCA Protein Assay (Thermo Fisher Scientific). Spectra were recorded in 1 mm path length quartz cells, between 195 and 250 nm at a scan speed of 100 nm per minute and 5 scans were signal averaged per sample. Data were baseline corrected and converted to mean residue ellipticity based on a mean molecular mass per residue of 110 Da. Plots were generated using Prism.

Liposomal cargo release assay

Stocks of 1,2-dioleoyl-*sn*-glycero-3-phosphocholine (DOPC, Avanti Polar Lipids) and 1,2-dioleoyl-*sn*-glycero-3-phospho-L-serine (sodium salt) (DOPS, Avanti Polar Lipids) were prepared in chloroform from dry powder. A lipid mixture of 80% DOPC and 20% DOPS was generated, freeze dried and hydrated with a solution of PBS containing the cargo, LANCE Eu-W1024 Biotin (PerkinElmer). The suspension was bath sonicated, freeze-thawed and extruded using Avanti Mini Extruder (Avanti Polar Lipids) fitted with a Nucleopore 0.1 µm membrane (Whatman) to yield large unilamellar vesicles. The liposomes were purified by eluting through a column packed with Pierce Streptavidin Agarose resin (Thermo Fisher Scientific). Cargo release assay was set up by mixing liposomes (1 µM in lipid concentration, diluted from 10 mM stock) with 0.5 mg ml^{-1} NINJ1 α-helix region peptide, its sequence-scrambled analogue (IAAAAMKMYLANSLEHAKSLKVVLASQDSE), or Melittin peptide (AnaSpec) (from 5 mg ml^{-1} stocks) in PBS buffer with 80 nM Streptavidin-Alexa Fluor 647 conjugate (Thermo Fisher Scientific). A set of background control samples was made with liposomes alone mixed with 5% DMSO in ddH_2O solution. All samples were loaded into wells of a ProxiPlate (PerkinElmer). TR-FRET readout was recorded on an EnVision 2105 multimode plate reader (PerkinElmer). The liposomes were then digested by adding 1% CHAPS to each well and 100% cargo release recorded. Results were converted to percentage cargo released per well and background control subtracted. Plot was generated using Prism.

C. rodentium infection

Female 12–14-week-old *Ninj1*$^{-/-}$ and littermate wild-type control mice were infected perorally with 2×10^9 CFU of log-phase cultured *C. rodentium* (ATCC 51459) after overnight fasting. Infected mice were monitored for survival for 17 days after infection. Plot was generated using Prism.

LPS septic shock

Mouse model of LPS-induced acute septic shock was performed as previously described[11,16,37]. In brief, male mice aged 8 to 10 weeks were injected intraperitoneally with 54 mg kg^{-1} LPS (*E. coli* O111: B4, Sigma) and monitored eight times daily for a total of 6 days. Plots were generated using Prism.

Statistics and reproducibility

Unless otherwise specified, results are representative of two independent experiments and means are of at least three individual replicates.

Reporting summary

Further information on research design is available in the Nature Research Reporting Summary linked to this paper.

Data availability

RNA-sequencing data are available through the Gene Expression Omnibus (GEO) database at accession number GSE156395. Datasets from UniProt database (https://www.uniprot.org/) including the mouse and contaminant subsets as well as the following accession numbers: Q70131, Q92982, P70617, F1PMB0, Q2TA30, R4GJU8, H9G4V3, Q66JI7, A0A0R4IDX9, Q9NZG7 and Q9JL89 were used. Other datasets generated during and/or analysed during the current study are available from the corresponding authors on reasonable request. Source data are provided with this paper.

31. Nelms, K. A. & Goodnow, C. C. Genome-wide ENU mutagenesis to reveal immune regulators. *Immunity* **15**, 409–418 (2001).
32. Kayagaki, N. et al. IRF2 transcriptionally induces *GSDMD* expression for pyroptosis. *Sci. Signal*. **12**, eaax4917 (2019).
33. Andrews, T. D. et al. Massively parallel sequencing of the mouse exome to accurately identify rare, induced mutations: an immediate source for thousands of new mouse models. *Open Biol*. **2**, 120061 (2012).
34. Murphy, J. M. et al. The pseudokinase MLKL mediates necroptosis via a molecular switch mechanism. *Immunity* **39**, 443–453 (2013).
35. Modzelewski, A. J. et al. Efficient mouse genome engineering by CRISPR-EZ technology. *Nat. Protocols* **13**, 1253–1274 (2018).
36. Aglietti, R. A. et al. GsdmD p30 elicited by caspase-11 during pyroptosis forms pores in membranes. *Proc. Natl Acad. Sci. USA* **113**, 7858–7863 (2016).
37. Kayagaki, N. et al. Noncanonical inflammasome activation by intracellular LPS independent of TLR4. *Science* **341**, 1246–1249 (2013).
38. Contrepois, K. et al. Cross-platform comparison of untargeted and targeted lipidomics approaches on aging mouse plasma. *Sci. Rep*. **8**, 17747 (2018).
39. Bakalarski, C. E. et al. The impact of peptide abundance and dynamic range on stable-isotope-based quantitative proteomic analyses. *J. Proteome Res*. **7**, 4756–4765 (2008).
40. Wang, G. G. et al. Quantitative production of macrophages or neutrophils ex vivo using conditional Hoxb8. *Nat. Methods* **3**, 287–293 (2006).
41. Wittig, I., Braun, H. P. & Schägger, H. Blue native PAGE. *Nat. Protocols* **1**, 418–428 (2006).
42. Waterhouse, A. et al. SWISS-MODEL: homology modelling of protein structures and complexes. *Nucleic Acids Res*. **46** (W1), W296–W303 (2018).
43. Ashkenazy, H., Erez, E., Martz, E., Pupko, T. & Ben-Tal, N. ConSurf 2010: calculating evolutionary conservation in sequence and structure of proteins and nucleic acids. *Nucleic Acids Res*. **38**, W529–W533 (2010).
44. Ashkenazy, H. et al. ConSurf 2016: an improved methodology to estimate and visualize evolutionary conservation in macromolecules. *Nucleic Acids Res*. **44**, W344–W350 (2016).
45. UniProt Consortium. UniProt: a worldwide hub of protein knowledge. *Nucleic Acids Res*. **47** (D1), D506–D515 (2019).
46. Sievers, F. et al. Fast, scalable generation of high-quality protein multiple sequence alignments using Clustal Omega. *Mol. Syst. Biol*. **7**, 539 (2011).
47. Robert, X. & Gouet, P. Deciphering key features in protein structures with the new ENDscript server. *Nucleic Acids Res*. **42**, W320-4 (2014).

Acknowledgements We thank the staff of the Australian Phenomics Facility, Genentech Transgenic Technology, imaging cores, and antibody engineering group, S. Wu, S. Gierke, F. Gallardo-Chang, Z. Altshuler and W. Fairbrother for technical expertise and discussion, K. Newton for manuscript editing, and W. Alexander for *Mlkl*$^{-/-}$ mice. Figures 2b, k, 3h were created with biorender.com.

Author contributions N.K., O.S.K., B.L.L., I.B.S., K.O., J.P., Z.M., V.C., T.D.A, L.X.M. and L.A.M. designed and performed experiments, Q.L. and W.S. performed secretome and lipidomics analysis, D.Y., J.K., M.X., J.Z., W.P.L. and B.S.M. performed in vivo studies, M.R.-G. generated the *Ninj1*$^{-/-}$ mice, G.U. performed the liposomal cargo release assay, O.S.K. and R.R. provided computational analysis, O.S.K., I.B.S., M.S. and J.D.W. performed microscopic analysis, and C.C.G., E.M.B. and V.M.D. contributed to experimental design. N.K. wrote the paper with input from all authors.

Competing interests N.K., O.S.K., B.L.L., I.B.S., K.O., Q.L., W.S., D.Y., J.K., M.X., J.Z., W.P.L., B.S.M., G.U., J.P., M.R.G., Z.M., R.R., M.S., J.D.B. and V.M.D. are all employees of Genentech Inc.

Additional information
Supplementary information The online version contains supplementary material available at https://doi.org/10.1038/s41586-021-03218-7.
Correspondence and requests for materials should be addressed to N.K. or V.M.D.
Peer review information *Nature* thanks the anonymous reviewers for their contribution to the peer review of this work.
Reprints and permissions information is available at http://www.nature.com/reprints.

a

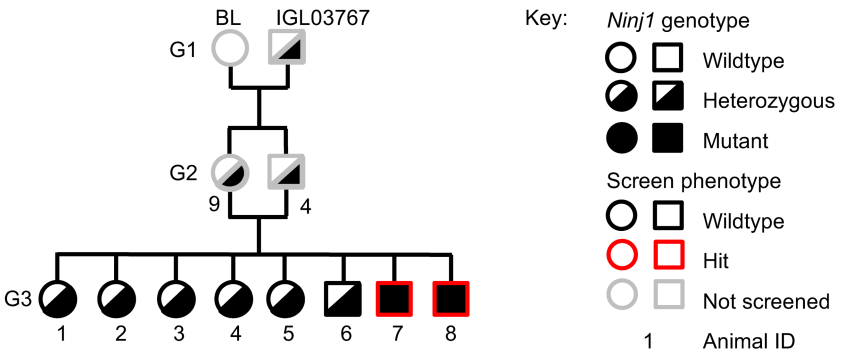

b

Chr	2	2	2	2	4	4	4	10	10	11	11	11	12	13	13	15	17	17	19
Gene	*Fcnb*	*Gm21985,Slc12a6*	*Cdan1*	*4933406J08Rik*	*Szt2*	*Ptchd2*	*Klhl17*	*Syn3,Timp3*	*Ppfia2*	*Myocd*	*Zzef1*	*Git1*	*Abcb5*	*Nid1*	*Ninj1*	*Krt84*	*Ring1*	*Mtcl1*	*Olfr1426*
Amimal																			
5	M	H	H	H	W	W	W	H	M	H	H	H	M	H	H	H	H	H	H
6	H	H	H	H	W	W	W	W	H	W	H	H	H	H	H	W	W	W	W
7	H	H	H	H	H	H	M	W	W	H	H	H	H	H	M	H	W	W	W
8	H	W	W	W	W	W	W	H	H	H	H	H	H	M	M	W	W	W	W

Key:

W	Wildtype
H	Heterozgyous
M	Mutant
	Assay hit
M	Assay hit and mutant

c

Extended Data Fig. 1 | Homozygosity of the *Ninj1* point mutation correlates with low responsiveness to LPS. a, *Ninj1* genotypes and screen phenotypes of mice derived from IGL03767. Identification numbers of screened mice are shown. G, generation. **b**, Nineteen SNV genotypes mutated in the pedigree and their phenotypes. **c**, Wild-type and IGL03767 *Ninj1* genes. Exon 2 coding sequence is in uppercase and SNV mutation is in bold and highlighted with an asterisk. Grey boxes represent exons.

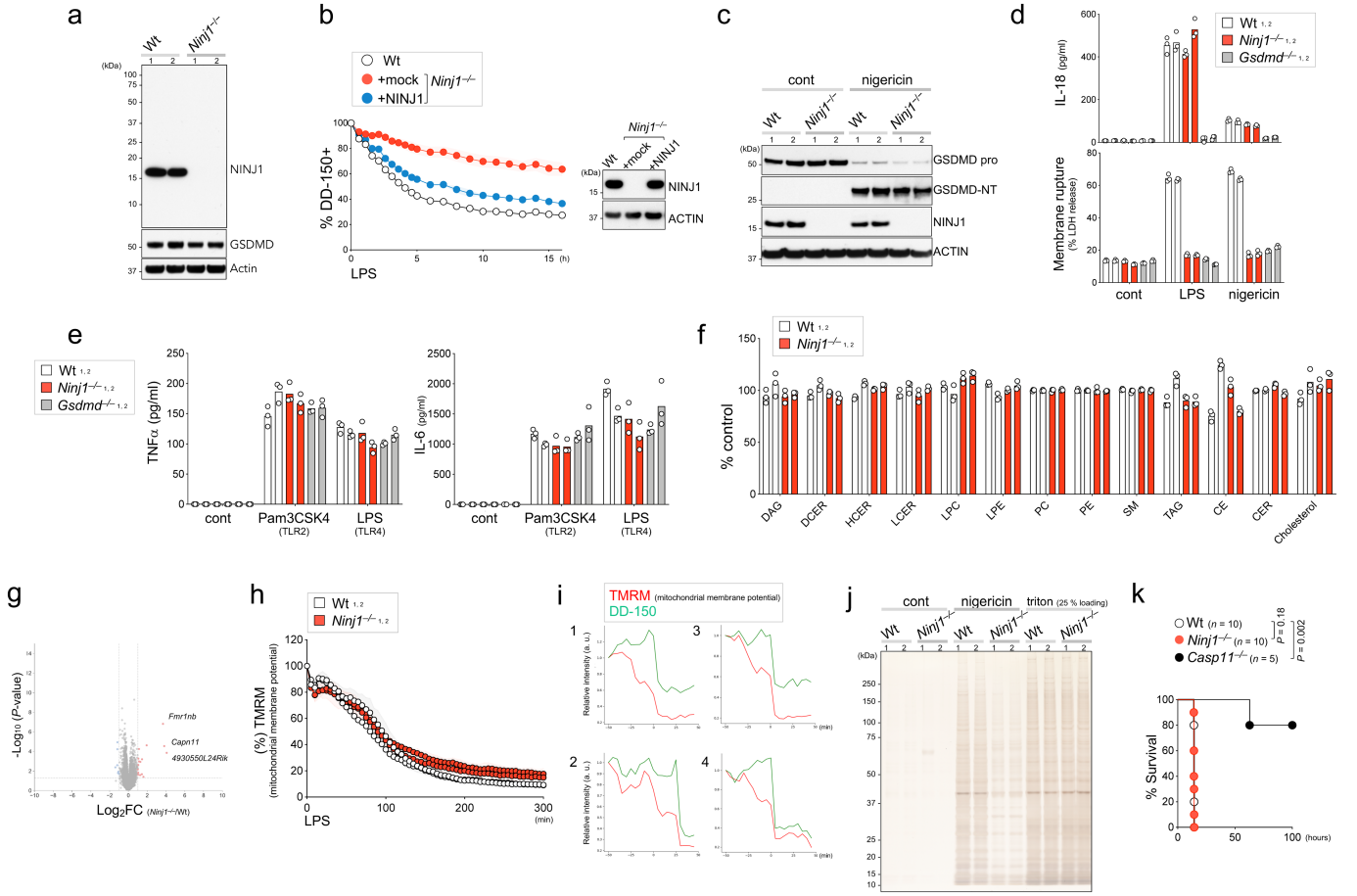

Extended Data Fig. 2 | NINJ1 is essential for pyroptosis-related PMR. **a**, Immunoblot of NINJ1 and GSDMD in BMDM lysates. **b**, Left, release of DD-150 in live-cell imaging analysis of iMACs after LPS electroporation over a 16-h time course. Right, immunoblot of NINJ1 in *Ninj1*$^{-/-}$ iMACs reconstituted with NINJ1. Data are means (circles) ± s.d. (shaded area) of three individual replicates. **c**, Immunoblot of GSDMD, GSDMD-NT and NINJ1 in supernatant and extract from nigericin-stimulated primed BMDMs. Actin is from a separate blot. **d**, LDH or IL-18 release from BMDMs stimulated as in Fig. 2d. **e**, IL-6 or TNF production from BMDMs stimulated with Pam3CSK4 (TLR2) or extracellular LPS (TLR4). **f**, Lipid composition of primed BMDMs. Lipids profiled are diacylglycerol (DAG), dihydroceramide (DCER), hexosylceramide (HCER), lactosylceramide (LCER), lysophosphatidylcholine (LPC), lysophosphatidylethanolamine (LPE), phosphatidylcholine (PC), phosphatidylethanolamine (PE), sphingomyelin (SM), triacylglycerol (TAG), cholesteryl ester (CE), and ceramide (CER). **g**, RNA-seq of primed BMDMs. **h**, Time-lapse imaging analysis of mitochondrial membrane potential as measured by tetramethylrhodamine methyl ester perchlorate (TMRM) in primed BMDMs following LPS electroporation. Data are means (circles) ± s.d. (shaded area) of three individual replicates. **i**, Single-cell time-lapse imaging analysis of TMRM and DD-150 release in primed wild-type BMDMs after LPS electroporation. Time point '0' corresponds to the point of maximal TMRM decline for each cell. **j**, Silver staining of proteins in culture supernatant of nigericin-stimulated primed BMDMs. **k**, Kaplan–Meier survival plots for mice challenged with 54 mg kg^{-1} LPS. *P* values were calculated by a two-sided Gehan–Breslow–Wilcoxon test. Unless otherwise specified, data are means (bars) of at least three individual replicates (circles). *n* = 2 per genotype. For gel source data, see Supplementary Fig. 1.

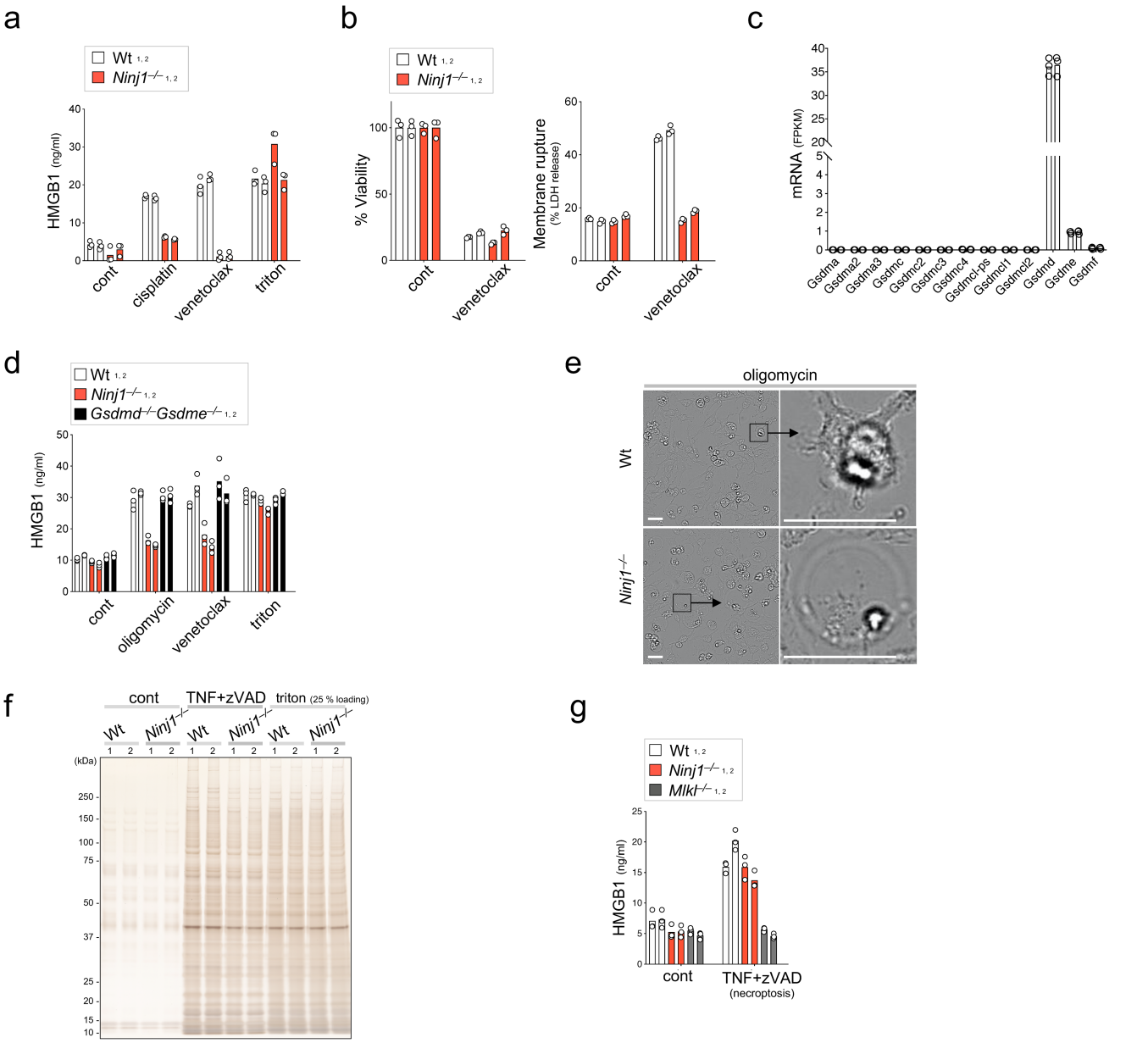

Extended Data Fig. 3 | NINJ1 has a global role in PMR induction related to pyroptosis, apoptosis and necrosis. a, **d**, **g**, Release of HMGB1 from BMDMs stimulated with cisplatin, venetoclax, oligomycin (**a**, **d**), or TNF plus zVAD (**g**). **b**, Viability (left) and LDH release (right) of venetoclax-stimulated BMDMs. **c**, Expression of indicated gasdermin transcripts in RNA-seq analysis of BMDMs. FPKM, fragments per kilobase of transcript per million mapped reads. **e**, Bright-field images of BMDMs cultured with oligomycin. Scale bars, 25 µm. **f**, Silver staining of proteins in culture supernatant of BMDMs stimulated with TNF and zVAD. Unless otherwise specified, data are means (bars) of at least three individual replicates (circles). $n = 2$ per genotype. For gel source data, see Supplementary Fig. 1.

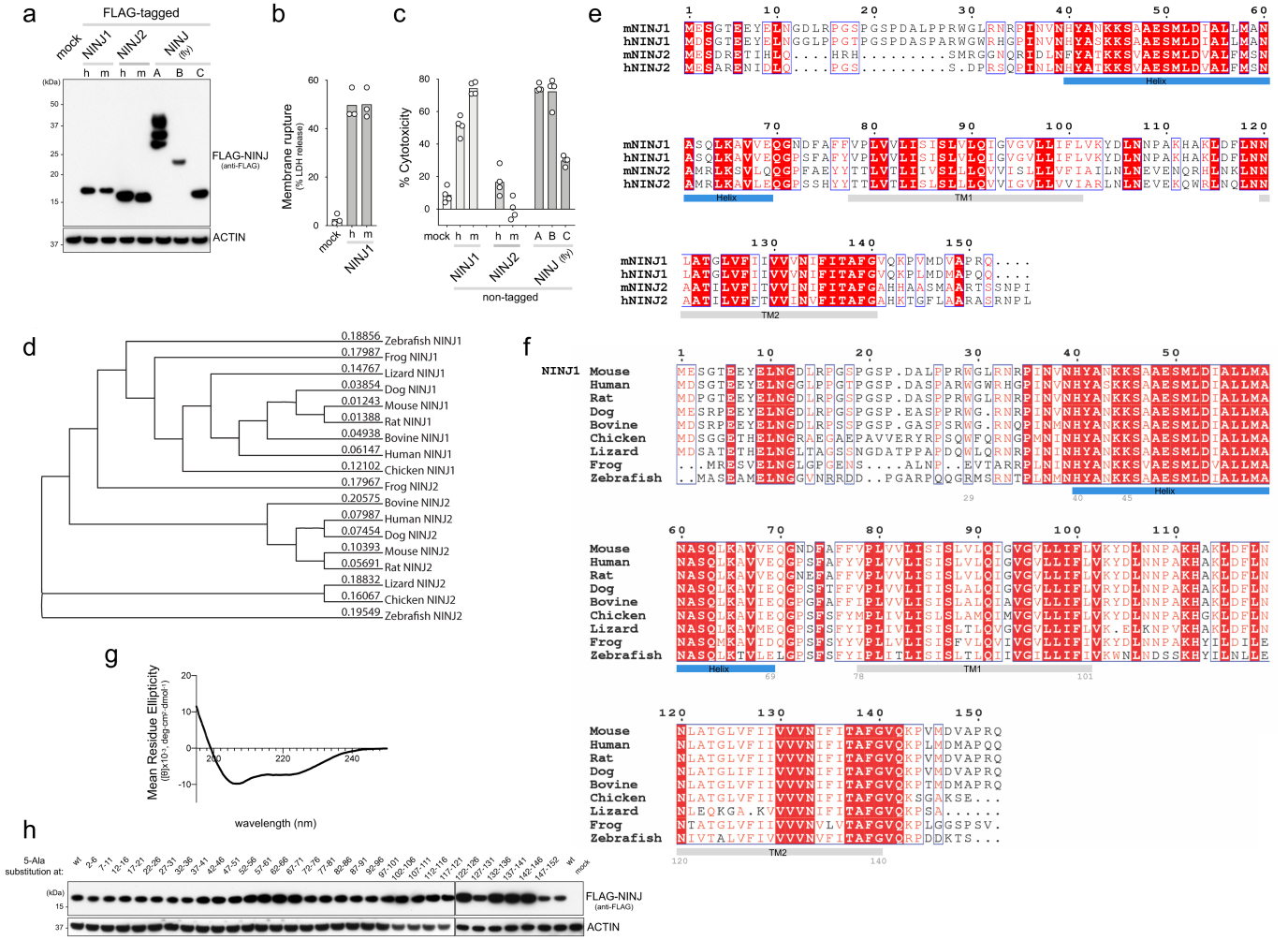

Extended Data Fig. 4 | Phylogenetic tree and amino acid sequence alignment of NINJ1 and NINJ2. a, Immunoblot of Flag–NINJ1 from Fig. 4a; representative of two independent experiments. **b**, LDH release from Flag–NINJ1 transfected HEK293T cells. Data are means (bars) of at least three individual replicates (circles) **c**, Cytotoxicity of non-tagged human and mouse NINJ1, NINJ2, and dNINJ-A, B, C in HEK293T cells. Data are means (bars) of at least four individual replicates (circles). **d**, Phylogenetic tree of NINJ1 and NINJ2. Numbers represent standardized distance scores (number of amino acid substitutions per length of the alignment). **e**, Multiple alignment of NINJ1 and NINJ2 amino acid sequences with the extracellular α-helix domain predicted by JPred highlighted in blue. **f**, Multiple alignment of NINJ1 amino acid sequences with the extracellular α-helix domain predicted by JPred. **g**, Circular dichroism spectra of NINJ1 α-helix region peptide that shows characteristic α-helix pattern (two dips at 208 nm and 222 nm). **h**, Immunoblot of Flag–NINJ1 from Fig. 4b; representative of two independent experiments. For gel source data, see Supplementary Fig. 1.

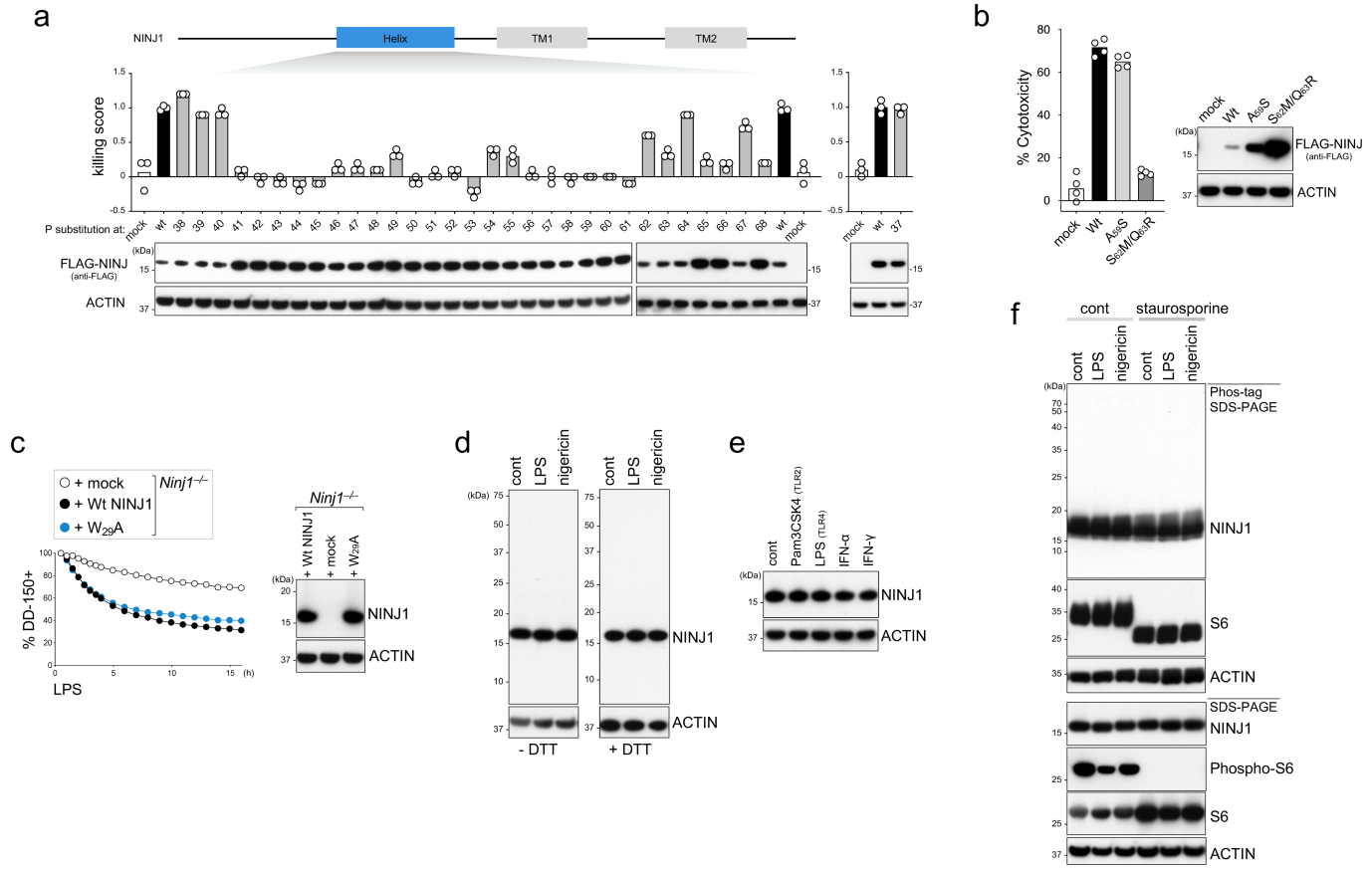

Extended Data Fig. 5 | Biochemical analysis of NINJ1. a, Top, NINJ1 domain structure. Middle, cytotoxicity of Flag-tagged wild-type NINJ1 or NINJ1 with proline point mutants in HEK293T cells. Numbers indicate positions of amino acid residues that were replaced by proline. Cytotoxicity (killing score) was normalized against wild-type NINJ1 control. Bottom, immunoblot of Flag–NINJ1. Data are means (bars) of at least three individual replicates (circles). **b**, Left, cytotoxicity of Flag-tagged wild-type NINJ1 or NINJ1 mutants in HEK293T cells. Right, immunoblot of Flag–NINJ1. Data are means (bars) of at least four individual replicates (circles). **c**, Left, release of DD-150 in live-cell imaging of *Ninj1*$^{-/-}$ iMACs reconstituted with NINJ1 after LPS electroporation. Right, immunoblot of iMACs with anti-NINJ1 polyclonal antibody. Data are means (circles) ± s.d. (shaded area) of three individual replicates. **d**, **e**, Immunoblot of NINJ1 in primed BMDMDs stimulated with LPS electroporation or nigericin (**d**), or in non-primed BMDMDs cultured with indicated stimuli (**e**). **f**, Phos-tag SDS–PAGE analysis of LPS electroporation- or nigericin-stimulated primed BMDMs with or without staurosporine pre-treatment. S6, ribosomal protein S6. Results in **d**–**f** are representative of two independent experiments. For gel source data, see Supplementary Fig. 1.

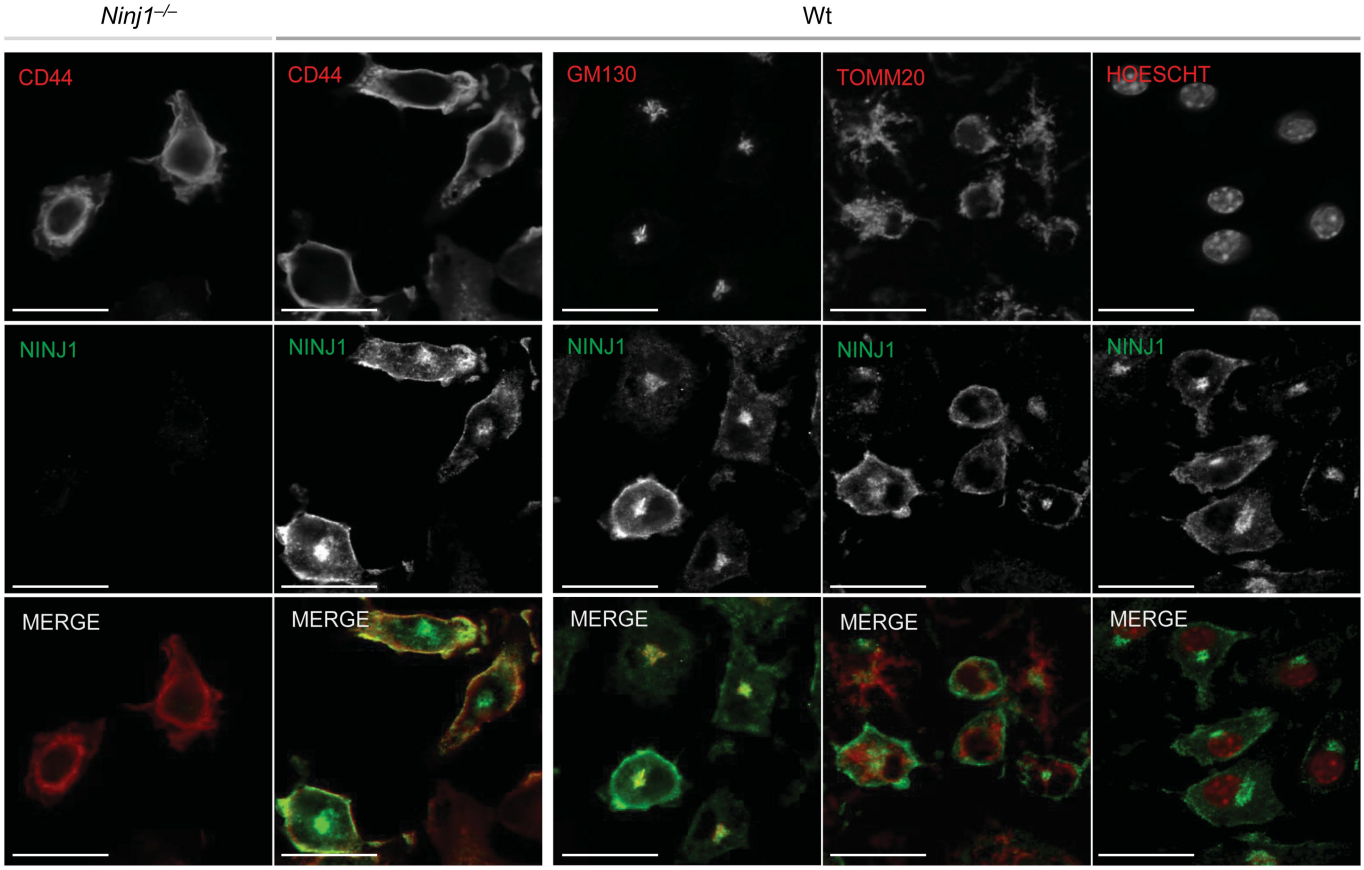

Extended Data Fig. 6 | Subcellular localization of NINJ1. Immunofluorescence microscopy of NINJ1 and indicated markers in primed BMDMs. Scale bars, 25 µm. Micrographs are representative of two independent experiments.

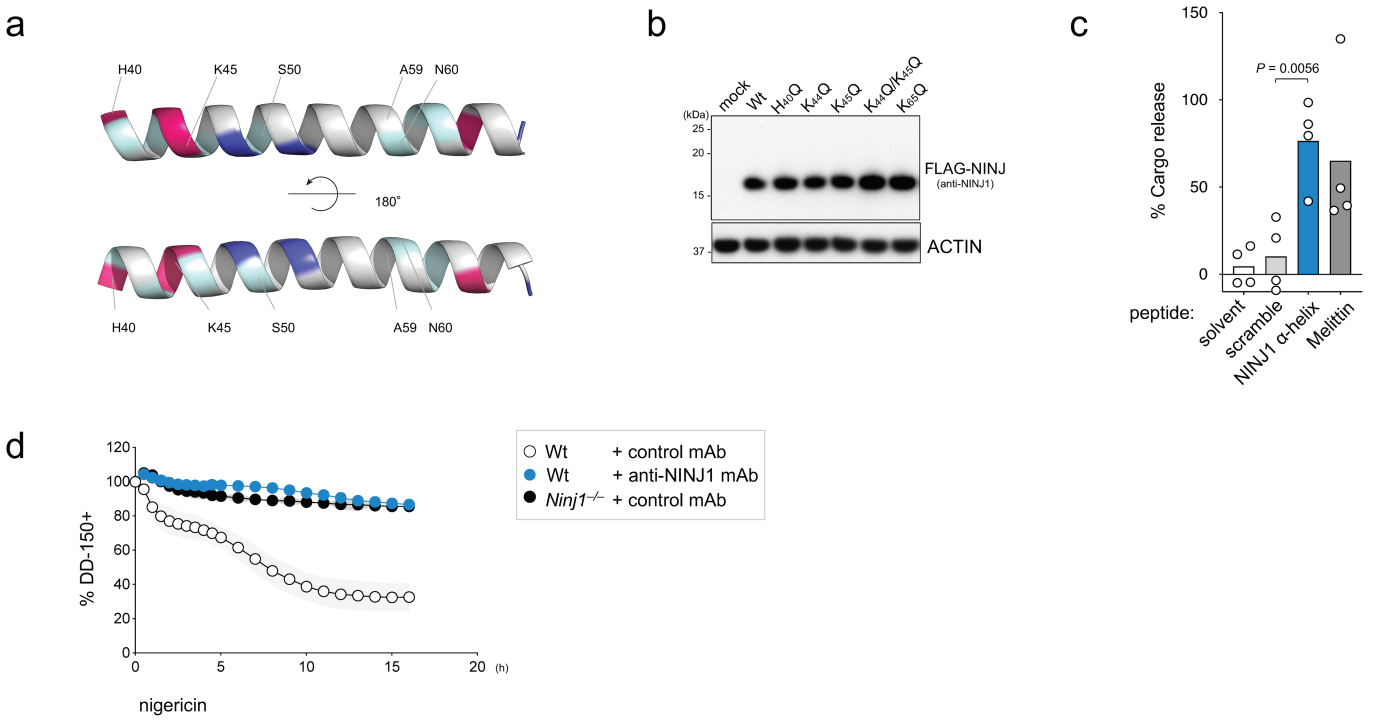

Extended Data Fig. 7 | Characterization of NINJ1 extracellular α-helix domain. a, Computational model of the NINJ1 extracellular domain. Grey, hydrophobic residues; blue, negatively charged residues; light blue, polar residues; red, positively charged residues. **b**, Immunoblot of Flag–NINJ1 in HEK293T cells from Fig. 4e; representative of two independent experiments. **c**, Liposome cargo release by the NINJ1 α-helix region peptide, its sequence scrambled variant, or Melittin (α-helical bee venom peptide). Data are means (bars) of four individual replicates (circles). *P* value was calculated using a two-tailed unpaired Student's *t*-test. **d**, Release of DD-150 in live-cell imaging of BMDMs after stimulation by nigericin in the presence of 20 μg ml^{-1} of indicated monoclonal antibodies. Data are means (circles) ± s.d. (shaded area) of four individual replicates. mAb, monoclonal antibody. For gel source data, see Supplementary Fig. 1.

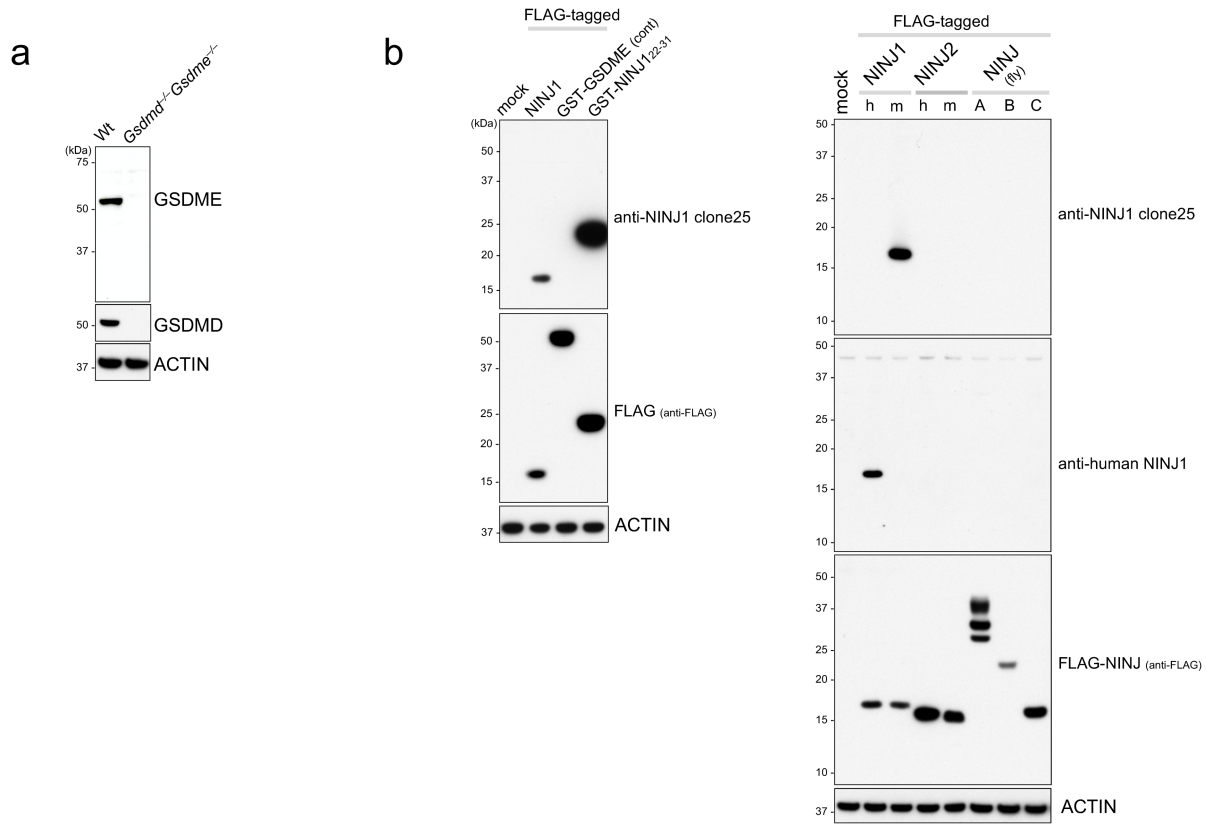

Extended Data Fig. 8 | Characterization of *Gsdmd*$^{-/-}$ *Gsdme*$^{-/-}$ BMDMs and anti-NINJ1 monoclonal antibody. a, Immunoblot of GSDME in BMDMs. GSDME is from a separate blot. **b**, Immunoblots with anti-mouse NINJ1 monoclonal antibody clone 25 in HEK293T cells transfected with the indicated Flag-tagged constructs. Results in **a** and **b** are representative of two independent experiments. For gel source data, see Supplementary Fig. 1.

Extended Data Table 1 | Bioinformatic analysis of ENU-induced SNVs present in IGL03767 pedigree

Chromosome	Coordinate (GRCm38)	Reference Base	Variant Base	Amino Acid Change	Splice Position	Polyphen Score	Polyphen Prediction	MGI Accession ID	Gene Name
2	28076801	T	C	N->S		0.68	possibly damaging	MGI:1341158	*Fcnb*
2	112351334	T	G	W->G		1	probably damaging	MGI:5439454, MGI:2135960	*Gm21985,Slc12a6*
2	120731501	T	A	M->L		0.839	possibly damaging	MGI:1916218	*Cdan1*
2	122198386	T	A	S->R		0.053	benign	MGI:1921651	*4933406J08Rik*
4	118384250	C	T	Disrupted splicing	6	N/A	N/A	MGI:3033336	*Szt2*
4	148241534	C	T	V->I		0.002	benign	MGI:2444403	*Ptchd2*
4	156233690	T	C	T->A		0.601	possibly damaging	MGI:2678948	*Klhl17*
10	86300975	G	C	Disrupted splicing	1	N/A	N/A	MGI:1351334, MGI:98754	*Syn3,Timp3*
10	106819492	A	G	T->A		0.005	benign	MGI:2443834	*Ppfia2*
11	65180944	T	C	Disrupted splicing	2	N/A	N/A	MGI:2137495	*Myocd*
11	72875126	T	A	I->N		0.001	benign	MGI:2444286	*Zzef1*
11	77505957	T	C	L->P		0	benign	MGI:1927140	*Git1*
12	118928695	T	C	D->G		0	benign	MGI:1924956	*Abcb5*
13	13476392	A	G	N->D		1	probably damaging	MGI:97342	*Nid1*
13	49193734	A	T	Disrupted splicing	2	N/A	N/A	MGI:1196617	*Ninj1*
15	101528735	T	G	D->A		0.998	probably damaging	MGI:96700	*Krt84*
17	34022575	T	C	D->G		0.093	benign	MGI:1101770	*Ring1*
17	66344319	C	T	V->I		0.001	benign	MGI:1915867	*Mtcl1*
19	12087993	A	T	D->E		0.317	benign	MGI:3031260	*Olfr1426*

Extended Data Table 2 | List of top hits from secretome analysis

Gene Symbol	Description	log2_fc	adj_pval
Plec	Plectin	-1.5735411	1.34E-66
Dync1h1	Cytoplasmic dynein 1 heavy chain 1	-1.7681909	4.49E-48
Flna	Filamin-A	-1.9976335	2.96E-42
Iqgap1	Ras GTPase-activating-like protein IQGAP1	-2.263248	3.65E-27
Psmd2	26S proteasome non-ATPase regulatory subunit 2	-2.2822816	6.34E-24
Sptan1	Spectrin alpha chain, brain	-2.0996548	1.7E-25
Hsp90aa1	Heat shock protein HSP 90-alpha	-2.3249883	1.48E-22
Rrbp1	Ribosome-binding protein 1	-1.6092643	1E-31
Tln1	Talin-1	-1.6212596	9.57E-30
Rnf213	Ring finger protein 213	-1.5767322	6.98E-29
Eif3a	Eukaryotic translation initiation factor 3 subunit A	-1.5972246	9.07E-26
Diaph1	Protein diaphanous homolog 1	-2.2650811	1.06E-17
Aars	Alanyl-tRNA synthetase, cytoplasmic	-2.1223791	7.17E-18
Tcp1	T-complex protein 1 subunit alpha	-2.0447724	1.81E-18
Smc2	Structural maintenance of chromosomes protein 2	-2.5042407	1.14E-14
Ap2m1	AP-2 complex subunit mu	-2.4305962	5.72E-15
Eif5b	Eukaryotic translation initiation factor 5B	-2.0962521	3.34E-17
Smc3	Structural maintenance of chromosomes protein 3	-2.6832107	2.35E-13
Actn4	Alpha-actinin-4	-2.6133402	2.2E-13
Lmna	Prelamin-A/C	-1.7880621	5.61E-19
Snx6	Sorting nexin-6	-2.5099778	3.43E-13
Stip1	Stress-induced-phosphoprotein 1	-1.7363794	2.25E-18
Hspa4	Heat shock 70 kDa protein 4	-1.8943487	3.42E-16
Cand1	Cullin-associated NEDD8-dissociated protein 1	-2.282329	6.36E-13
Cse1l	Exportin-2	-3.0024777	5.61E-10
Sptbn1	Spectrin beta chain, brain 1	-1.8489119	2.4E-15
Lars	Leucyl-tRNA synthetase, cytoplasmic	-2.7938336	2.31E-10
Slk	STE20-like serine/threonine-protein kinase	-1.9956628	5.01E-14
Eprs	Bifunctional aminoacyl-tRNA synthetase	-2.1459888	7.87E-13
Psmd6	26S proteasome non-ATPase regulatory subunit 6	-3.2169063	9.38E-09

Secretome analysis of released proteins in culture supernatant of primed BMDMs stimulated by LPS electroporation (Fig. 2i) *P* values were calculated using a two-sided linear mixed-effects model.

nature research

Corresponding author(s): Nobuhiko Kayagaki and Vishva M. Dixit

Last updated by author(s): Dec 20, 2020

Reporting Summary

Nature Research wishes to improve the reproducibility of the work that we publish. This form provides structure for consistency and transparency in reporting. For further information on Nature Research policies, see our Editorial Policies and the Editorial Policy Checklist.

Statistics

For all statistical analyses, confirm that the following items are present in the figure legend, table legend, main text, or Methods section.

n/a	Confirmed	
☐	☒	The exact sample size (*n*) for each experimental group/condition, given as a discrete number and unit of measurement
☐	☒	A statement on whether measurements were taken from distinct samples or whether the same sample was measured repeatedly
☐	☒	The statistical test(s) used AND whether they are one- or two-sided *Only common tests should be described solely by name; describe more complex techniques in the Methods section.*
☒	☐	A description of all covariates tested
☒	☐	A description of any assumptions or corrections, such as tests of normality and adjustment for multiple comparisons
☐	☒	A full description of the statistical parameters including central tendency (e.g. means) or other basic estimates (e.g. regression coefficient) AND variation (e.g. standard deviation) or associated estimates of uncertainty (e.g. confidence intervals)
☐	☒	For null hypothesis testing, the test statistic (e.g. *F*, *t*, *r*) with confidence intervals, effect sizes, degrees of freedom and *P* value noted *Give P values as exact values whenever suitable.*
☒	☐	For Bayesian analysis, information on the choice of priors and Markov chain Monte Carlo settings
☒	☐	For hierarchical and complex designs, identification of the appropriate level for tests and full reporting of outcomes
☒	☐	Estimates of effect sizes (e.g. Cohen's *d*, Pearson's *r*), indicating how they were calculated

Our web collection on statistics for biologists contains articles on many of the points above.

Software and code

Policy information about availability of computer code

Data collection	Imaging (live and fixed) data captured using MetaXpress 6.5.4.532, Slidebook 6, and Incucyte S3 2019A.
Data analysis	Mass spectrometry data analysed using Mascot 2.4.1, the Vista Algorithm 4.0.0, and TIBCO Spotfire 7.8.0 HF-003. Plots were generated either with Prism 7.0 or Matplotlib 3.1.3. Imaging data analysed and prepared using scikit-image 0.16.2 and Imaris 9.5. Secondary structure prediction was performed using the JPred 4 server. Structure modeling was performed with SWISS-MODEL 2018 and visualized with PyMOL 2.3.5. Conservation score was calculated using the ConSurf 2016 server. Sequence alignment and phylogenetic tree creation were performed using Clustal Omega 1.2.4. Sequence alignment was visualized with ESPript 3.0. RNA sequencing data analysed using GSNAP 2013-11-01 and voom/limma R package 3.44.3 (as described in the methods).

For manuscripts utilizing custom algorithms or software that are central to the research but not yet described in published literature, software must be made available to editors and reviewers. We strongly encourage code deposition in a community repository (e.g. GitHub). See the Nature Research guidelines for submitting code & software for further information.

Data

Policy information about availability of data

All manuscripts must include a data availability statement. This statement should provide the following information, where applicable:

- Accession codes, unique identifiers, or web links for publicly available datasets
- A list of figures that have associated raw data
- A description of any restrictions on data availability

RNA-sequencing data is available through the GEO database (GSE156395). Source Data for Figs. 1–4 and Extended Data Figs. 2–8 are provided with the paper. Datasets from UniProt database (https://www.uniprot.org/) including the mouse and contaminant subsets as well as the following accession numbers: Q70131,

Q92982, P70617, F1PMB0, Q2TA30, R4GJU8, H9G4V3, Q66JI7, A0A0R4IDX9, Q9NZG7, and Q9JL89 were used. Other datasets generated during and/or analysed during the current study are available from the corresponding authors on reasonable request.

Field-specific reporting

Please select the one below that is the best fit for your research. If you are not sure, read the appropriate sections before making your selection.

☒ Life sciences ☐ Behavioural & social sciences ☐ Ecological, evolutionary & environmental sciences

For a reference copy of the document with all sections, see nature.com/documents/nr-reporting-summary-flat.pdf

Life sciences study design

All studies must disclose on these points even when the disclosure is negative.

Sample size	No sample size calculations were performed. Cells from at least 2 animals per genotype were analysed for reproducibility. This sample size was chosen to match previously published work by our group (Kayagaki et al, Nature 2015; Lee et al, J. Exp. Med. 2018, Kayagaki et al, Sci. Signal.). Due to the low variability between wild-type animals in in these vitro experiments, this sample size is also widely accepted in the field. To account for greater variability, in vivo survival studies (C. rodentium infection and LPS septic shock) utilized greater sample sizes as guided by previously published work (Kayagaki et al, Nature 2015).
Data exclusions	No data were excluded from analyses.
Replication	Whenever possible, readouts were performed with at least 2 animals per genotype. All attempts at replication were successful.
Randomization	Groups were determined by genotype rather than treatment, therefore, randomization was not applicable.
Blinding	Imaging was performed blindly and automatically using an ImageXpress Micro Confocal or Incucyte system. For other experiments, mice and cell lines were picked and treated by the same individual, so blinding to genotype and treatment as well as during data collection and analysis was not possible.

Reporting for specific materials, systems and methods

We require information from authors about some types of materials, experimental systems and methods used in many studies. Here, indicate whether each material, system or method listed is relevant to your study. If you are not sure if a list item applies to your research, read the appropriate section before selecting a response.

Materials & experimental systems

n/a	Involved in the study
☐	☒ Antibodies
☐	☒ Eukaryotic cell lines
☒	☐ Palaeontology and archaeology
☐	☒ Animals and other organisms
☒	☐ Human research participants
☒	☐ Clinical data
☒	☐ Dual use research of concern

Methods

n/a	Involved in the study
☒	☐ ChIP-seq
☒	☐ Flow cytometry
☒	☐ MRI-based neuroimaging

Antibodies

Antibodies used	Antibodies used for western blots were from Genentech (17G2G9 anti-GSDMD used at 0.2 ug/mL; 25 anti-NINJ1 used at 0.2 ug/mL, polyclonal anti-mouse NINJ1 used at 1 ug/mL; polyclonal anti-mouse GSDME used at 0.5 ug/mL), Cell Signaling Technology (anti-mouse cleaved GSDMD, cat#50928S, lot#1 used at 1 ug/mL; 5G10 anti-S6 ribosomal protein, cat#2217S, lot#7 used at 1 ug/mL; D57.2.2E anti-phospho-S6 ribosomal protein (Ser235/236), cat#4858S, lot#6 used at 1 ug/mL), Novus Biologicals (AC-15 anti-beta-actin HRP, cat#NB600-501H, lot#109M4849V-022020-H used at 0.1 ug/mL;, anti-human NINJ1, cat#NBP1-59210, lot#QC16583-42972 used at 1 ug/mL), MilliporeSigma (anti-FLAG M2 HRP, cat#A8592, lot#SLCF0816 used at 1 ug/mL), and Jackson Immunoresearch (HRP-anti-rat, cat#112-035-175; HRP-anti-rabbit, cat#111-035-047, lot#129784; HRP-anti-rabbit, cat#111-035-046, lot#129872; all diluted 1/5000). Antibodies used for immunofluorescence were from MilliporeSigma (2F8.1 TOMM20, cat#MAB166, lot#3403466 diluted 1/100), Abcam (KM201 anti-CD44, cat#ab25340, lot#GR3291624-2 diluted 1/500), BD Biosciences (clone 35 GM130, cat#610823, lot#8352796 diluted 1/100), and Invitrogen (AF488 anti-rabbit, cat#A32731, lot#VC297825 diluted 1/500; AF647 anti-rat, cat#A21247, lot#2156534 diluted 1/500; A647 anti-mouse, cat#A3278, lot#UK290265 diluted 1/500).
Validation	- 17G2G9 anti-GSDMD was validated for WB using wild-type and GSDMD-/- BMDMs in Aglietti et al (2016) Proc Natl Acad Sci USA 113(28):7858-63

- Clone 25 anti-NINJ1 antibody was validated for WB by comparing lysates from wild-type and NINJ1-/- BMDMs (Fig 2c, this study)
- Polyclonal anti-mouse NINJ1 antibody was validated for WB by comparing lysates from NINJ1-/- iMACs with an empty vector and a WT NINJ1 vector (Extended Data Fig 5c, this study)
- Polyclonal anti-mouse GSDME was validated for WB by comparing lysates from wild-type and GSDMD-/-GSDME-/- BMDMs (Extended Data Fig 8a, this study)
- anti-mouse cleave GSDMD (cat#50928S, lot#1 Cell Signaling Technology, used at 1 ug/mL). The antibody guarantee covers the use of the antibody for WB applications. https://www.cellsignal.com/products/primary-antibodies/cleaved-gasdermin-d-asp276-antibody-mouse-specific/50928
-5G10 anti-S6 ribosomal protein (cat#2217S, lot#7 Cell Signaling Technology, used at 1 ug/mL). The antibody guarantee covers the use of the antibody for WB applications. The antibody has been referenced in 1087 publications. https://www.cellsignal.com/products/primary-antibodies/s6-ribosomal-protein-5g10-rabbit-mab/2217?site-search-type=Products&N=4294956287&Ntt=2217s&fromPage=plp&_requestid=105901
-D57.2.2E anti-phospho-S6 ribosomal protein (Ser235/236) (cat#4858S, lot#6 Cell Signalling Technology, used at 1 ug/mL). The antibody guarantee covers the use of the antibody for WB applications. The antibody has been referenced in 640 publications. https://www.cellsignal.com/products/primary-antibodies/phospho-s6-ribosomal-protein-ser235-236-d57-2-2e-xp-rabbit-mab/4858
-AC-15 anti-beta-actin HRP (cat#NB600-501H, lot#109M4849V-022020-H Novus Biologicals, used at 0.1 ug/mL). The antibody guarantee covers the use of the antibody for WB applications. The antibody has been referenced in 8 publications. https://www.novusbio.com/products/beta-actin-antibody-ac-15_nb600-501h#reviews-publications
-anti-human NINJ1 (cat#NBP1-59210, lot#QC16583-42972 Novus Biologicals, used at 1 ug/mL). The antibody guarantee covers the use of the antibody for WB applications. https://www.novusbio.com/products/ninjurin-1-antibody_nbp1-59210
-anti-FLAG M2 HRP (cat#A8592, lot#SLCF0816 MilliporeSigma, used at 1 ug/mL). The antibody guarantee covers the use of the antibody for WB applications. The antibody has been referenced in 1006 publications. https://www.sigmaaldrich.com/catalog/product/sigma/a8592?lang=en&region=US
-anti-TOMM20, clone 2F8.1 (cat#MABT166, lot#3403466 MilliporeSigma diluted 1/100). The antibody guarantee covers the use of the antibody for immunocytochemistry applications. The antibody has been referenced in 2 publications. https://www.sigmaaldrich.com/catalog/product/mm/mabt166?lang=en&region=US
-anti-CD44, clone KM201 (cat#ab25340, lot#GR3291624-2 Abcam, diluted 1/500). The antibody has been referenced in 20 publications. https://www.abcam.com/cd44-antibody-km201-ab25340.html
-anti-GM130, clone 35 (cat#610823, lot#8352796 BD Biosciences, diluted 1/100). The antibody guarantee covers the use of the antibody for immunofluorescence applications. The antibody has been referenced in 5 publications.

Eukaryotic cell lines

Policy information about cell lines

Cell line source(s)	293T cells (ATCC CRL-3216), ER-Hoxb8 immortalized macrophages (derived from Ninj1-/- C57BL6/N and wild-type littermate mice as described in methods, Genentech)
Authentication	Cells not authenticated
Mycoplasma contamination	Cells negative for mycoplasma.
Commonly misidentified lines (See ICLAC register)	Not used.

Animals and other organisms

Policy information about studies involving animals; ARRIVE guidelines recommended for reporting animal research

Laboratory animals	All mice (Mus musculus) were maintained on a C57BL/6N genetic background with the exception of ENU mutagenized mice that were of C57BL/6NCrl background. Strains included Ninj1-/- (this study), Ninj1mt/mt (this study, Figure 1d), caspase-11-/- (Kayagaki et al . 2011 Nature 479(7371):117-21), Gsdmd-/- (Kayagaki et al . 2015 Nature 526:666-671), Gsdmd-/-Gsdme-/- (this study), Mlkl-/- (Murphy et al. 2013 Immunity 39:443-453), and 129X1/SvJ (Kayagaki et al. 2011 Nature 479:117-121). For C. rodentium study, 12-14 week old female mice were used. For LPS study, 8-10 week old male mice were used. For in vitro studies, mice of both sexes between 5 to 10 weeks old were used. Mice were housed in individually ventilated cages within animal rooms maintained on a 14:10-hour, light:dark cycle. Animal rooms were temperature and humidity-controlled, between 68-79°F and 30-70% respectively, with 10 to 15 room air exchanges per hour.
Wild animals	The study did not involve wild animals.
Field-collected samples	The study did not involve samples collected from the field.
Ethics oversight	For ENU-mutagenized mouse strains, all animals used were cared for and used in experiments approved by the Australian National University Animal Experimentation Ethics Committee under protocol A2018/07. For all other animal studies, all animal procedures were conducted under protocols approved by the Genentech Institutional Animal Care and Use Committee in an Association for Assessment and Accreditation of Laboratory Animal Care (AAALAC)-accredited facility in accordance with the Guide for the Care and Use of Laboratory Animals and applicable laws and regulations.

Note that full information on the approval of the study protocol must also be provided in the manuscript.